14 January 2000

To: Distribution
From: John Kessler (EPRI)

Subject: Transmittal of EPRI report, "Colloid Transport and Deposition in Water-Saturated and Unsaturated Sand and Yucca Mountain Tuff", EPRI TR-110546

Enclosed is a copy of the report. If you need additional copies, or know of others not on the distribution list who would like a copy, please let me know.

Sincerely,

John Kessler

John H. Kessler
Manager, HLW Repository Issue Resolution Program

Distribution:

Joonhong Ahn, University of California - Berkley (1)
Tae Ahn, U.S. NRC (3)
Ralph Anderson, Nuclear Energy Institute (1)
Bob Andrews, Duke Engineering Services, Inc. (5)
Florence Ardorino, Electricite de France (1)
Bill Arnold, Sandia National Lab (1)
Bob Baca, Center for Nuclear Waste Regulatory (2)
William D. Barnard, Nuclear Waste Technical Review (5)
Michael Bauser, Morgan, Lewis & Bockius LLP (1)
David Bennett, Galson Sciences, Ltd. (1)
Allen Benson, U.S. Department of Energy (1)
James A. Blink, Lawrence Livermore National Lab (1)
David Bodansky, University of Washington (1)
Gudmunder Bodvarsson, Lawrence Berkley National (1)
Les Bradshaw, Nye County (1)
Stephan Brocoum, U.S. Department of Energy (1)
Robert Budnitz, Future Resources Associates, Inc. (1)
Dan Bullen, Iowa State University (1)
Andrew Campbell, U.S. NRC. (1)
Dwayne Chestnut, LLNL, c/o CRWMS M&O (1)
Raymond Clark, U.S. Environmental Protection (2)
Richard Codell, U.S. NRC (1)
Jared Cohon, U.S. Waste Technical Review Board (1)
Kevin Coppersmith, Geomatrix Consultants, Inc. (1)
Thomas Cotton, (1)
Ian Crossland, NIREX (1)
John Czarnecki, U.S. Geological Survey (1)
Claude Degueldre, Paul Scherrer Institute (1)
Holly Dockery, Sandia National Laboratories (3)
F. Stanley Echols, Winston & Straw (1)
Mohamed El-Genk, University of New Mexico (1)
Norman Eisenberg, U.S. NRC (1)
Leif Eriksson, COMPA Industries, Inc. (1)
Christophe Eripret, Electricite de France (1)
Charles Fairhurst, (1)
James Firth, U.S. NRC (1)
Steve Frischman, Nuclear Waste Project Office (2)
J.H. Gauthier, Sandia National Laboratories (1)
Philippe Giaume, Electricite de France (1)
April Gil, U.S. Department of Energy (1)
Chad Glenn, U.S. NRC (1)
Giorgio Gnugnoli, U.S. NRC (1)
Richard Goffi, Booz-Allen & Hamilton, Inc. (1)
Jean-Marie Gras, Electricite de France (2)
Harris Greenberg, YMSCO (1)
John Greeves, U.S. NRC (2)
William Halsey, Lawrence Livermore National Lab (1)
Carol Hanlon, (1)
Ahmed Hasan, Sandia National Laboratories (1)
Alan Hooper, NIREX (1)
George Hornberger, University of Virginia (1)
James Houseworth, Duke Engineering Services, Inc. (1)

Distribution *(continued)*:

Rob Howard, Duke Engineering Services, Inc. (1)
James Hunt, University of California - Berkley (1)
Mikael Jensen, Swedish Radiation Protection Inst. (1)
G.L. Johnson, JAI Corporation (1)
Andrew Kadak, Kadak Associates, Inc. (1)
Annie Kersting, Lawrence Livermore National Lab (1)
Thomas E. Kiess, Board on Radioactive Waste Mgmt. (1)
Martha Kohler, Lawrence Livermore National Lab (1)
Janet Kotra, U.S. NRC (1)
Matthew Kozak, Monitor Scientific LLC (1)
Steve Kraft, Nuclear Energy Institute, (1)
Donald Langmuir, HSC (1)
Howard Larson, U.S. NRC (1)
Jan van der Lee, U.S. NRC (1)
Mike Lee, U.S. NRC
Linda Lehman, T&REGI (1)
Bret Leslie, U.S. NRC (1)
Gordon Linsley, International Atomic Energy Agency (1)
R. Loux, State of Nevada (1)
Pierre-Laurent Lucille, Electricite de France (1)
Miguel Lugo, TRW Environmental Safety Sys. Inc. (1)
Abraham Van Luik, U.S. Department of Energy (2)
Tim McCartin, U.S. NRC (2)
Keith McConnell, U.S. NRC (2)
Rod McCullum, Nuclear Energy Institute (1)
Laura McDowell-Boyer (1)
Maureen McGraw, Los Alamos National Lab (1)
Robin McGuire, Risk Engineering, Inc. (1)
Annemarie Meike, Lawrence Livermore National Lab (1)
Srikanta Mishra, Duke Engineering & Services, Inc. (1)
Henri Mouney, Electricite de France (1)
M. Naito, Power Reactor & Nuclear Fuel Dvlp. Corp. (1)
Claudia Newberry, U.S. Department of Energy (1)
W. Mark Nutt, Golden Federal Services (1)
Tonis Papp, SKB (1)
Russell Patterson, U.S. Department of Energy (1)
Claudio Pescatore, OECD Nuclear Energy Agency (1)
Mark Peters, Los Alamos Nat'l Lab (2)
Christophe Poinssot, CEA (1)
Rob Rechard, Sandia Nat'l Lab (1)
Phillip Reed, U.S. NRC (1)
Paul Reimus, Los Alimos Nat'l Lab (2)
Leon Reiter, NWTRB (1)
Dennis Richardson, Morrison Knudsen Corp. (2)
Lawrence Rickertsen, TRW Environmental Safety Sys. (1)
Budhi Sagar, Center for Nuclear Waste Regulatory (3)
David Sassani, Duke Engineering & Services, Inc. (1)
Steven Saterlie, TRW Environmental Safety Sys. (1)
Joy Schwartz (1)
Graham Smith, QuantiSci, Ltd. (1)
Christine Stockman, Los Alimos Nat'l Lab (2)
Ray Stout, Lawrence Livermore Nat'l Lab (1)
Dean Stucker, Yucca Mountain Site Office (1)
Ed Sudicky, University of Waterloo (1)
Trevor Sumerling, Safety Assesment Mgmt., Ltd. (1)
Eileen Supko, Energy Resources International, Inc. (1)
W.C. Thurber, S. Cohen and Associates, Inc. (1)
Engelbrecht von Tiesenhausen, Clark County (1)
Ines Triay, Los Alimos Nat'l Lab (1)
Mark Tynan, U.S. Dept. of Energy (2)
Carlos Torres Vidal, International Atomic Energy (1)
Stratis Vomvoris, NAGRA (1)
Ray Wallace, USGS (1)
Chris Whipple, ICF Kaiser Engineers, Inc. (1)
Dennis Williams, U.S. Dept. of Energy (1)
Michael Wilson, Sandia Nat'l Lab (1)
Paul Witherspoon (1)
Gordon Wittmeyer, Southern Research Institute (1)
Andrew Wolfsberg, Los Alimos Nat'l Lab (1)
Yu-Shu Wu, Lawrence Berkley Nat'l Lab (1)
Ray Wymer (1)
Jean Yonker, TRW Environmental Safety Sys., Inc. (1)
Wei Zhou, Monitor Scientific LLC (1)
P. Zuidema, NAGRA (1)
Eric Zwahlen, Golden Federal Services (1)
George Zyvoloski, Los Alimos Nat'l Lab (1)

T Ahn

EPRI

Colloid Transport and Deposition in Water-Saturated and Unsaturated Sand and Yucca Mountain Tuff

Effect of Ionic Strength and Moisture Saturation

Colloid Transport and Deposition in Water-Saturated and Unsaturated Sand and Yucca Mountain Tuff

Effect of Ionic Strength and Moisture Saturation

TR-110546

Final Report, December 1999

EPRI Project Manager
J. Kessler

EPRI • 3412 Hillview Avenue, Palo Alto, California 94304 • PO Box 10412, Palo Alto, California 94303 • USA
800.313.3774 • 650.855.2121 • askepri@epri.com • www.epri.com

DISCLAIMER OF WARRANTIES AND LIMITATION OF LIABILITIES

THIS DOCUMENT WAS PREPARED BY THE ORGANIZATION(S) NAMED BELOW AS AN ACCOUNT OF WORK SPONSORED OR COSPONSORED BY THE ELECTRIC POWER RESEARCH INSTITUTE, INC. (EPRI). NEITHER EPRI, ANY MEMBER OF EPRI, ANY COSPONSOR, THE ORGANIZATION(S) BELOW, NOR ANY PERSON ACTING ON BEHALF OF ANY OF THEM:

(A) MAKES ANY WARRANTY OR REPRESENTATION WHATSOEVER, EXPRESS OR IMPLIED, (I) WITH RESPECT TO THE USE OF ANY INFORMATION, APPARATUS, METHOD, PROCESS, OR SIMILAR ITEM DISCLOSED IN THIS DOCUMENT, INCLUDING MERCHANTABILITY AND FITNESS FOR A PARTICULAR PURPOSE, OR (II) THAT SUCH USE DOES NOT INFRINGE ON OR INTERFERE WITH PRIVATELY OWNED RIGHTS, INCLUDING ANY PARTY'S INTELLECTUAL PROPERTY, OR (III) THAT THIS DOCUMENT IS SUITABLE TO ANY PARTICULAR USER'S CIRCUMSTANCE; OR

(B) ASSUMES RESPONSIBILITY FOR ANY DAMAGES OR OTHER LIABILITY WHATSOEVER (INCLUDING ANY CONSEQUENTIAL DAMAGES, EVEN IF EPRI OR ANY EPRI REPRESENTATIVE HAS BEEN ADVISED OF THE POSSIBILITY OF SUCH DAMAGES) RESULTING FROM YOUR SELECTION OR USE OF THIS DOCUMENT OR ANY INFORMATION, APPARATUS, METHOD, PROCESS, OR SIMILAR ITEM DISCLOSED IN THIS DOCUMENT.

ORGANIZATION(S) THAT PREPARED THIS DOCUMENT

Pacific Northwest National Laboratory
Washington State University, Tri-Cities

ORDERING INFORMATION

Requests for copies of this report should be directed to the EPRI Distribution Center, 207 Coggins Drive, P.O. Box 23205, Pleasant Hill, CA 94523, (800) 313-3774.

Electric Power Research Institute and EPRI are registered service marks of the Electric Power Research Institute, Inc. EPRI. POWERING PROGRESS is a service mark of the Electric Power Research Institute, Inc.

Copyright © 1999 Electric Power Research Institute, Inc. All rights reserved.

CITATIONS

This report was prepared by

Pacific Northwest National Laboratory
K6-81, P.O. Box 999
Richland, WA 99352

Presently at:

Westinghouse Savannah River Co.
Building 773-43a, Room 215
Aiken, SC 29808

Principal Investigator
D. Kaplan

Washington State University, Tri-Cities
2710 University Drive
Richland, WA 99352

Principal Investigator
A. Gamerdinger

This report describes research sponsored by EPRI.

The report is a corporate document that should be cited in the literature in the following manner:

Colloid Transport and Deposition in Water-Saturated and Unsaturated Sand and Yucca Mountain Tuff: Effect of Ionic Strength and Moisture Saturation, EPRI, Palo Alto, CA, 1999. TR-110546.

REPORT SUMMARY

Colloid-aided radionuclide transport has been considered a potentially important mechanism for the candidate spent fuel and high level waste (HLW) repository at Yucca Mountain. This mechanism, however, has not been treated in Yucca Mountain Total System Performance Assessments (TSPAs) until recently. Even then there has been little discussion of possible colloid retention in the unsaturated zone. This report summarizes investigations of potential colloid retention in sand and Yucca Mountain tuff as a function of ionic strength and degree of saturation. The work suggests that colloid retention in the Yucca Mountain system is likely to occur due to sufficiently high ionic strength of the groundwater composition. For saturations of less than about 60%, colloid retention also becomes increasingly important.

Background

Most TSPAs of radionuclide transport away from HLW repositories via groundwater only consider dissolved (aqueous) radionuclide species. When aqueous species alone are considered, specific radionuclides such as plutonium become relatively unimportant because they are largely insoluble and readily sorb onto a range of geologic materials. However, if radionuclides are characterized as colloids (particles no larger than a few microns) rather than aqueous waste forms, then the situation becomes less clear for species such as plutonium. Previous research has shown that colloids do not obey the same transport "rules" as aqueous species and may, in fact, move faster through geologic materials in the colloidal form than in the dissolved phase. Furthermore, while colloids definitely exist in waste repositories, what remains uncertain, is their significance to radionuclide migration.

Objectives

To conduct scoping experiments to determine if colloid transport is likely under ionic strength and moisture saturation conditions similar to those at the candidate Yucca Mountain HLW repository.

Approach

Investigators conducted experiments to determine colloid mobility through fully and partially saturated porous media. As the basis for these experiments, they used colloids, water chemistries, and porous media resembling those predicted during near- to long-term HLW storage beneath Yucca Mountain. Polystyrene latex microspheres with surface properties similar to many natural colloids and radiocolloids were passed through columns of sand or crushed Yucca Mountain tuff in an ultracentrifuge device capable of maintaining a wide partial saturation range. Investigators measured retention within the column as a function of porous media type (sand or Yucca Mountain tuff), ionic strength, and degree of saturation. In addition, they varied the ionic strength of the "J-13" groundwater composition, collected near Yucca Mountain, in a range of 0-10x. Moisture saturations investigated ranged from 11-100%.

Results

Colloid retention in the columns increased dramatically when the critical coagulation concentration (CCC)—the solute concentration at which colloid attachment begins to proceed rapidly—was reached (about 5x J-13). Colloid retention in a fully saturated column at 1x J-13 ionic strength was about 10% over a distance of ~7 cm, indicating that sufficient ionic strength exists in J-13 to rapidly reduce suspended colloid concentrations downstream of the candidate repository. When the partial saturation was reduced to below 60%, colloid retention in the 7 cm column increased substantially.

These results suggest that radionuclides associated with colloids are unlikely to travel very far beneath the candidate repository at Yucca Mountain. Ionic strength plays the dominant role in reducing colloid mobility, with partial saturation playing an increasingly important role as saturation values decrease below about 60%. Consequently, TSPA "credit" for limited colloid mobility in partially saturated fractures will likely be justifiable in performance assessment calculations following research directed at this well-defined problem.

Finally, another important implication of this work is that processes occurring in unsaturated systems cannot always be simply scaled from observations of saturated systems. This is certainly true of the effect of ionic strength on colloid mobility. In this study, irrespective of ionic strength, no colloid deposition (100% colloid recovery) was observed. In the 11-17% saturated systems, ionic strength had a significant effect on colloid removal, suggesting an interactive effect on colloid deposition between ionic strength and saturation. These underscore the limitations of extrapolating processes occurring in saturated conditions to unsaturated conditions.

EPRI Perspective

EPRI has been active in the development of TSPAs for the proposed spent-fuel and HLW repository at Yucca Mountain. However, recent TSPA considerations of colloid-aided transport have assumed highly mobile colloids in the absence of experimental data. This report was commissioned to provide input to EPRI and others on the potential relevance of colloid-aided transport in the Yucca Mountain system. The ultimate objective is to establish, quantitatively and reasonably—without being overly conservative—the extent to which colloid-aided transport is (or is not) an important mechanism for the Yucca Mountain system. Related EPRI work includes the following: Study of Unsaturated Zone Flow and Transport Models of Fractured Tuff (TR-108536, October 1998); Colloids in Saturated and Partially Saturated Porous Media: Approaches to the Treatment of Colloids in Yucca Mountain Total System Performance Assessments (TR-112135, April 1999); and Alternative Approaches to Assessing the Performance and Suitability of Yucca Mountain for Spent Fuel Disposal (TR-108732, November 1998).

TR-110546

Keywords

Yucca Mountain
High-level radioactive wastes
Radionuclide migration

EXECUTIVE SUMMARY

Ramsay (1988) reviewed the role of colloids in the release of radionuclides from nuclear waste repositories. He pointed out that colloids may enhance the source term and the transport rate away from the waste form. The source term is increased because the radionuclides may leave the waste form not only in the dissolved phase, but also in the colloidal phase. The transport rate is increased because some radionuclides may move faster through geologic materials in the colloidal than dissolved phase (reviewed by McCarthy and Zachara [1989]). The most poignant conclusions Ramsay made is that there is little uncertainty that colloids exist in waste repositories; what remains uncertain, is the significance of these colloids on radionuclide migration.

This research focused on defining limiting conditions for colloid transport in subsurface porous media. Colloid mobility and deposition were determined in model systems consisting of quartz sand or tuff (stationary solid collected from the Topopah Spring member at Yucca Mountain), latex microspheres (colloidal particles), and solutions of simulated Yucca Mountain groundwater. The experimental conditions selected for these experiments were based upon conditions reported to exist at Yucca Mountain. The ionic strength of the aqueous solution was manipulated as a first-step in defining limiting chemical conditions for colloid transport at the site of the proposed Yucca Mountain nuclear waste repository. Solutions of 0x (deionized water), 0.1x, 1x, and 10x the ionic strength of simulated J-13 groundwater were used under steady-state flow conditions. The ionic strength of simulated J-13 groundwater was 11.6 mol m^{-3}. For each series of experiments, water content was maintained at either 100%, 58-61%, or 11-18% moisture saturation. The colloid transport experiments were conducted using a centrifuge method, which creates uniform unsaturated conditions in porous media through the use of a flow-through centrifuge unit.

Results from saturated column experiments with "conservative" (non-interacting) tracers indicated reliable column performance and stable hydrodynamic conditions. Ionic strength had no effect on retardation, retention, or dispersion of the tracers. Colloid deposition followed a linear trend with increasing ionic strength and colloid deposition was effectively modeled as a pseudo-first-order process. Colloids were completely mobile in the 0x and 0.1x J-13 solutions, i.e., all of the colloids that were introduced into the columns were recovered in the effluent. At higher ionic strengths, a greater fraction of the colloids were deposited on the porous media over the ~7-cm length of the column: 11-13% for 1x; and 90% or more for 10x J-13. Multiple and replicate experiments were performed on the same column without altering colloid deposition or changing column hydrodynamics. The results were similar for the sand and tuff materials, suggesting that solution chemistry is a dominant factor in determining colloid mobility and deposition in water-saturated porous media.

At approximately 60% moisture saturation, mobility and retention were similar to saturated systems. However, with further desaturation to 11% and 17% for sand and tuff, respectively, mobility of the colloids decreased to a greater extent than was observed for 60% and 100% saturation. Deposition on the sand increased to approximately 15% for 0x, 20% for 0.1x, and 51% for 1x synthetic J-13 groundwater. Retention was greatest on the tuff at 17% moisture saturation: 37% for 0x, 42% for 0.1x, 74% for 1x and 89% for 10x. Colloid mobility is substantially reduced by (i) increasing ionic strength by a factor of 10, or (ii) decreasing moisture saturation to less than 20%. Based on the results of the settling experiments and determination of the critical coagulation concentration (CCC—the maximum salt concentration of the aqueous phase before colloid coagulation occurs), it seems likely that coagulation is the mechanism for colloid removal during transport at 10x synthetic J-13. Reduced moisture saturation had very little effect on colloid transport at this high ionic strength because removal was likely due to coagulation. The reduced moisture saturation had a greater impact on transport at the lower ionic strength conditions of 0x and 0.1x. The increase colloid retention in the tuff, as compared to the sand, can be attributed to the slightly smaller size of the tuff particles and to its coarser surface and more angular shape.

This research demonstrates colloid mobility in saturated and unsaturated sediments. Deposition on quartz sand and tuff increased with increasing ionic strength, with approximately 90% removal from solution with a 10-fold increase in ionic strength for synthetic J-13 groundwater. The results for deposition during transport were consistent with colloid removal from solution, i.e., a CCC equivalent to five times the ionic strength of J-13 water (or 58mol m^{-3}). Colloid transport in relatively dry sediments (i.e., < 20% moisture saturation) was not predicted from behavior in saturated or partially desaturated sediments (i.e., greater than or equal to ~60% moisture saturation). Decreased colloid mobility in unsaturated, as compared to saturated, systems has often been attributed to decreased film thickness of the water layer flowing over the matrix surfaces.

The results from these studies conducted under model conditions have several important implications regarding colloid transport at Yucca Mountain. First and foremost, colloid transport at Yucca Mountain will be greatly limited by the ionic strength of the groundwaters. In the near-field, the ionic strength will very likely exceed the critical coagulation concentration of the colloids . This will not permit the colloids to remain in suspension for transport. Even in the most dilute solutions that the colloids would be expected to encounter at the site, as estimated by J-13 water, only a fraction of the colloids (which varied with saturation), were found to travel through 7-cm column.

Another important implication of this work is that moisture content considerations alone will likely not limit colloid mobility in the porous tuff material, but may limit colloid mobility along the fractured tuff surfaces at Yucca Mountain. This is because the studies show that above 60% saturation, there was no observable moisture saturation effect on colloid mobility. Such high saturation levels are characteristic of the porous tuff while lower saturations may occur along the fractured surfaces of Yucca Mountain. These studies suggest that colloid mobility along these surfaces may be limited. Consequently, "credit" for limited colloid mobility in partially saturated fractures will likely be justifiable in performance assessment calculations once research directed at this well-defined problem is performed.

Finally, another important implication of this work is that processes that occur in unsaturated systems can not always be simply scaled from observations of saturated systems. This is certainly true of the effect of ionic strength on colloid mobility. In this study, irrespective of ionic strength, no colloid deposition (100% colloid recovery) was observed. In the 11 to 17% saturated systems, ionic strength had a significant effect on colloid removal, suggesting an interactive effect on colloid deposition between ionic strength and saturation. The cause for this interaction may be attributed to the double layer (electrostatic halo) of the colloid and matrix surfaces accounting for an increasing proportion of the total water volume as the degree of saturation decreases. Furthermore, it appears that at extreme desaturation ($\leq$ ~11% under these experimental conditions) or ionic strength ($\geq$~58 mol m^{-3}) that colloid mobility is controlled by the limiting factor and not the interaction of the two parameters. This research underscores the limitations of extrapolating processes occurring in saturated conditions to unsaturated condition. Additionally, this research indicates the importance of both physical and chemical system properties in determining colloid mobility and transport in subsurface sediments.

CONTENTS

1 INTRODUCTION **1-1**

Mineralogy, Hydrology and Water Chemistry at Yucca Mountain 1-1

Colloid Studies at the Nevada Test Site and Yucca Mountain 1-3

Colloid Mobility Under Unsaturated Conditions 1-4

Effect of Ionic Strength on Colloid Mobility Through Porous Media 1-6

Hypothesis and Objectives 1-6

Theory 1-7

Colloid Aggregation and Colloid Deposition 1-7

DLVO Forces 1-8

Critical Coagulation Concentration (CCC) 1-11

2 EXPERIMENTAL RESULTS **2-1**

Materials 2-1

Particle Characterization 2-4

Gravitational Settling and Critical Coagulation Concentration 2-5

Transport Method for Saturated Columns 2-5

Transport Method for Unsaturated Columns 2-7

3 RESULTS **3-1**

Particle Characterization 3-1

Gravitational Settling and Critical Coagulation Concentration 3-5

Transport Experiments in Saturated Columns 3-5

Conservative Tracer Transport 3-9

Colloid Transport and Retention 3-11

Transport Experiments in Unsaturated Columns 3-14

Conservative Tracer Transport 3-18

Colloid Transport and Retention 3-19

4 REFERENCES **4-1**

LIST OF FIGURES

Figure 1-1 Example of Interparticle Potential Plots Displaying Dispersion, Coagulation, and Slow Flocculation Based on DLVO Calculations 1-10

Figure 2-1 Scanning electron micrographs of the crushed tuff (top) and quartz (bottom) used as matrix material in this study. The quartz was slightly larger and appreciably smoother than the crushed tuff. 2-2

Figure 2-2 X-ray diffraction scan of the crushed tuff material (Topopah Spring) used in this study 2-3

Figure 3-1 Zeta Potential of 280-nm Latex Particles as a Function of Synthetic J-13 Groundwater Concentration and Ionic Strength (Vertical Lines Represent Standard Deviation of 12 Values) 3-2

Figure 3-2 Interpartical Potential as a Function of Separation Distance and Ionic Strength (Based on Equations 6 through 10 and Input Values in Table 3-1) 3-4

Figure 3-3 Primary Energy Barrier as a Function of Ionic Strength. Regression and 2σ Confidence Limits of the Regression Analysis are Presented 3-4

Figure 3-4 Second-Order Rate Constants and Sticking Coefficients as a Function of Ionic Strength. Regression Analysis was Conducted for data < 58 mol m^{-3}, the Approximate Critical Flocculation Concentration 3-6

Figure 3-5 Non-interactive Tracer Transport in Quartz Sand 3-10

Figure 3-6 Non-interactive Tracer Transport in Yucca Mountain Tuff 3-10

Figure 3-7 Transport and Deposition of 280 nm Colloids in Quartz Sand 3-12

Figure 3-8 Transport and Deposition of 280 nm Colloids in Yucca Mountain Tuff 3-13

Figure 3-9 Colloid Deposition during Transport in Sand and Tuff 3-14

Figure 3-10 Non-interactive Tracer Transport in Quartz Sand at 61% and 11% Moisture Saturation 3-18

Figure 3-11 Non-interactive Tracer Transport in Yucca Mountain Tuff at 71% and 17% Moisture Saturation 3-19

Figure 3-12 Transport and Deposition of 280 nm Colloids in Quartz Sand at 61% Moisture Saturation 3-20

Figure 3-13 Transport and Deposition of 280 nm Colloids in Tuff at 58% Moisture Saturation 3-20

Figure 3-14 Transport and Deposition of 280 nm Colloids in Quartz Sand at 11% Moisture Saturation 3-21

Figure 3-15 Transport and Deposition of 280 nm Colloids in Tuff at 17% Moisture Saturation 3-21

LIST OF TABLES

Table 2-1 Ionic Strength and Average pH of Aqueous Solutions Used in Transport Experiments 2-3

Table 2-2 Experimental conditions used in saturated and unsaturated colloid transport studies 2-6

Table 3-1 Input Values Used in DLVO Calculations 3-3

Table 3-2 Experimental Conditions and Parameters for Conservative Tracer Transport in Saturated Sand (S) and Tuff (T) Columns 3-7

Table 3-3 Experimental Conditions and Parameters for Colloid Transport in Saturated Sand (S) and Tuff (T) Columns 3-8

Table 3-4 Column Effluent pH for Selected Colloid Transport Experiments 3-9

Table 3-5 Definition of Dimensionless Transport Parameters (after Toride et al., 1995) 3-11

Table 3-6 Experimental Conditions and Parameters for Conservative Tracer Transport in Unsaturated Sand (S) and tuff (T) Columns 3-15

Table 3-7 Experimental Conditions and Parameters for Colloid Transport in Unsaturated Sand (S) and tuff (T) Columns 3-16

1
INTRODUCTION

Ramsay (1988) reviewed the role of colloids in the release of radionuclides from nuclear waste repositories. He pointed out that colloids may enhance the source term and the transport rate away from the waste form. The source term is increased because the radionuclides may leave the waste form not only in the dissolved phase, but also in the colloidal phase. The transport rate is increased because some radionuclides may move faster through geologic materials in the colloidal than dissolved phase (reviewed by McCarthy and Zachara [1989]). Perhaps one of the most poignant conclusions Ramsay made is that there is little uncertainty that colloids exist in waste repositories; what is uncertain, is the significance of these colloids on radionulcide migration.

Evaluating the potential threat of colloid-facilitated transport of radionuclides at Yucca Mountain is especially difficult due to the complexity and uncertainty associated with the geometry of the fractured system and the extremely long period of concern, tens of thousands of years. To address this issue, researchers and policy people generally evaluate experiments that attempt to approximate well-defined aspects of this complex problem. One aspect that has not been studied adequately is the movement of colloids through unsaturated porous or fractured systems. This area of research has been neglected because of the lack of an adequate experimental technique to evaluate it.

Mineralogy, Hydrology and Water Chemistry at Yucca Mountain

A brief review of the mineralogy, hydrology and water chemistry at Yucca Mountain is presented in this section. In-depth reviews are presented by Meijer (1990) and Triay et al. (1994). The mineralogy of a site affects colloid mobility in a number of ways. Minerals that tend to form small colloids will be more likely to create mobile colloids, e.g., smectites are smaller than illites/micas and for that reason tend to be more mobile. Minerals that are less soluble release less salts into the nearby water, thereby maintining lower ionic strength in the water and permitting colloids to remain in suspension. Finally, minerals of higher surface charge, such as smectites and illites/micas, tend to remain in suspension longer than minerals of lower surface charge, such as feldspars and quartz. Yucca Mountain tuffs consist primarily of feldspar and quartz (Bish and Vaniman 1985). The zeolites, clinoptilolite and mordenite, are abundant in parts of some nonwelded units (e.g., Calico Hills) but are limited to sparse fracture lining minerals in most of the devitrified tuffs. Clays (e.g., smectites, illites/micas) are locally abundant in the matrix of some tuffs, but are a minor component (1 to 3%) in most of the tuffs beneath the potential repository (Chipera and Bish 1989). Calcite is generally a minor component in the tuffs located between 300 and 900 m depths. It exists in higher concentration, 5 to 10%, in tuffs located <300 m and >900 m from the ground surface. Hematite is widely distributed as a trace mineral.

The mineralogy and geometry along the fractures are especially important for colloid transport because it will be these minerals that may contribute to the pool of mobile colloids and will directly interact as the immobile phase with mobile colloids. Meijer (1990) reviewed previous characterization work on fracture minerals. Manganese minerals were found in fractures throughout most of the holes. Calcite abundance along fractures followed a similar distribution as described above; it was more abundant above a 300-m depth and below a 900-m depth. Clays and zeolites abundance generally increased with depth, being the dominant secondary minerals in the lower parts of the holes. Silica and iron oxide/oxyhydroxide phases were unevenly distributed in fractures.

Total surface areas of three tuff samples from Yucca Mountain varied greatly, ranging from 2.6 and 10.0 m^2/g (BET; Meijer 1990). These surface areas values appear large when considering that sand-size particles have a surface areas between 0.1 to 1 m^2/g. It is likely that the heterogeneity of the surface area in Yucca Mountain is extremely large, being greatest in porous media and lowest in large fractured media.

The tuff surrounding the proposed spent fuel and HLW repository at Yucca Mountain contains intact, porous matrix interspersed with fractures and faults (DOE, 1998). The properties of both the matrix and fractures/faults is variable, but evidence suggests that groundwater flow is predominately in the system of connected, higher permeability fractures (DOE, 1998). For example, depending on the degree of welding and other textural features, the tuff units have matrix porosities in the range of 5 to 40%, and average matrix hydraulic conductivities in the range of 10^{-8} to 10^{-11} ms^{-1} (TRW, 1995). However, the presence of fracture zones increases the bulk rock permeability to values in the range of 10^{-5} to 10^{-7} ms^{-1} (TRW, 1995). Other than during periods of increased recharge from storms, water in the partially-saturated zone is located mostly within the matrix of the rocks, rather than in the fractures, because of matrix capillary effects (TRW, 1995). Field studies have shown that the porous tuff is almost completely saturated, with volumetric saturation levels (saturation is the percent of pore space occupied by water) well above 60% in all cases, except in elevated-temperature systems. However, the matrix porosity is generally characterized by rather small pore size distributions that would make significant colloid transport through the intact tuff difficult at best. Because of the episodic nature of flow in the fractures, saturation levels in the fractures are also likely to be temporally variable. This may be of considerable importance when attempting to understand the role of partial saturation in hindering colloid transport.

The chemical composition of the groundwater in the present and future groundwater flow systems will affect colloid transport. The plume chemistry is expected to change as it migrates from the near-field where engineered barriers will control water chemistry, to the far-field, where the site natural mineralogy will control water chemistry. Among the various materials that could retard waste movement are glass and cement. Glass leachate is typically high in pH (pH 10 to 12), sodium, carbonate, silica, and hydroxide. Cement leachate is typically high in pH, calcium, carbonate, and hydroxide. The ionic strength of these leachate can vary greatly but commonly range between 1 to 0.01 (Mann 1998). As the contaminant plume migrates into the far field, its background chemistry will approach that of the nearby uncontaminated groundwater. Using the groundwater chemistry of the Yucca Mountain area presented by Meijer (1992), one would expect the far field chemistry to be dilute sodium bicarbonate. Sodium, calcium, potassium, and magnesium are the major cations; bicarbonate, sulfate and chloride are the major anions in order of decreasing concentration. The only other water constituent is silica. The pH ranges from 6.5

to 9.4, but is typically 7 to 8. In the partially-saturated zone, pH is typically in the range of 6.4 to 7.5. The redox status is expected to be oxidizing with respect to Fe(II), and the ionic strength is ~0.01.

Colloid Studies at the Nevada Test Site and Yucca Mountain

A brief review of colloid characteristics and selected colloid studies are presented below. More in-depth reviews are provided by Triay et al. (1994), who compiled brief summaries of previous colloid studies, and Bennett et al. (1999), who provided a critical review of approaches to the treatment of colloids in Yucca Mountain TSPA.

In the Nevada Test Site, Kingston and Whitbeck (1991) sampled 24 springs and wells and reported that most of the groundwaters studied had colloid concentrations in the range from 0.28 to 1.35 mg/L; three sites had high colloid concentrations ranging from 6.48 to 25 mg/L. They also reported that no obvious correlation existed between water chemistry and colloid concentrations in the groundwater. The mineral composition of the colloids was remarkably similar, being composed of silica and relatively small amounts of clay and zeolite. Calcite was also detected in some of the samples. They concluded that colloids could travel through the Nevada Test Site subsurface based on their observation that colloids were ubiquitously present at similar concentrations and similar size distributions. It could be argued that these colloids are not necessarily traveling throughout the site but are being generated by similar local immobile material.

In addition to natural colloids, anthropogenic colloids may be derived from the waste itself or from repository construction and sealing materials. Bates et al. (1993) demonstrated that colloids are generated during waste glass dissolution and that the colloids generated often contain radioactive elements. Similarly, Feng et al. (1993) concluded that waste glass can contribute to the formation of colloids by 1) increasing ionic strength of the groundwater with leads to nucleation, 2) releasing radionuclides that form pseudocolloids (groundwater colloids with sorbed radionuclides), and 3) by spalling fragments of colloidal size from the surface layer of the reacted glass. Feng et al. (1993) reported that these colloids consisted of smectites and uranium silicates.

Choppin (1988) pointed out the importance of humic materials on metal ion speciation. Minai et al. (1992) measured total organic carbon concentrations in J-13 of 0.01 to 0.1 mg/L. They concluded that radionuclides with +3 oxidation states, such as Am, would be appreciably more inclined to form organic complexes that may enhance their mobility than uranyl.

Water from Well J-13 at the Nevada Test Site had a >0.45-μm colloid concentration of ~3 x 10^{-5} g/L and <0.45- to >0.005-μm colloid concentration of ~3 x 10^{-6} g/L (Ogard 1987). Based on these results, Ogard (1987) concluded that the particulates in the J-13 well water would have to exhibit a sorption distribution coefficient (Kd) greater than 4,000,000 mL/g for a given radionuclide in order for pseudocolloids (colloids in which radionuclides are sorbed to naturally occurring geological colloids) to contribute more than 10% to the total amount of radionuclide migration through Yucca Mountain. A Kd value of 4,000,000 mL/g essentially is limited to irreversible sorption processes, such as Cs to illitic minerals, or to sparingly soluble precipitation (heterogeneous precipitation onto a mineral surface).

Buddemeier and Hunt (1988) conducted ultrafiltration studies on groundwater samples collected from the Cheshire event located at the Nevada Test Site. They sampled the cavity created by the Cheshire event and fractured lava and tuff 300-m down-gradiuent from the cavity. A substantial concentration of submicron colloids and significant radionuclide concentration were found at both locations. A significant fraction of the radioactivity at both locations could be filtered (0.003-μm filters), suggesting they were associated with colloids. Many lanthanide and transition metal radionuclides were 100% filterable. Buddemeier and Hunt (1988) concluded that both the dissolved and colloidal radionuclide species migrated through the fractured system at the study site and that the radionuclides were strongly sorbed onto the colloids.

Kersting et al. (1999) recently reported that field studies suggested that plutonium migrated in association with colloids at the Nevada Test Site. The $^{240}Pu/^{239}Pu$ isotope ratio of the samples established that an underground nuclear test 1.3 km north of the sample site was the origin of the plutonium. They argued that colloidal groundwater migration must have played an important role in transporting the plutonium. Some uncertainty still remains regarding whether the experimental evidence provided in Kersting et al. (1999), in fact, provides indisputable evidence of colloid-facilitated plutonium transport. This uncertainty was recently reiterated in response to a Migration 99 presentation describing updates on this research program (Kersting and Brachmann 1999). Among the concerns expressed were that no evidence was provided that dissolved plutonium did not precipitate from solution while being pumped up from a depth of ~1300-m (redox changes are theoretically expected to exist between 1300 m and ground level). Another concern was that the difference between the calculated distance that the plutonium moved as a result of the initial explosion (200 to 300-m) and the observed distance (1300 m) is relatively quite small, less than an order of magnitude. It may be possible that the accuracy of the explosion model can not differentiate between these two distances, especially in fractured media, and that the recovered colloidal plutonium, in fact, was transported as part of the original explosion. A final concern is that it may be possible that the dissolved plutonium migrated to the sample site, where the well provides a conduit to surface air, and then precipitated to form colloidal material. Importantly, these concerns do not dismiss the possibility that colloids enhanced plutonium transport at the study site. Instead they question whether the field and laboratory evidence is sufficient to implicate colloids as the factor responsible for the apparent enhanced transport.

Colloid Mobility Under Unsaturated Conditions

Our present understanding of colloid transport in unsaturated systems is primarily based on results obtained from experiments conducted in saturated systems. The reason for this is, in part, because the experimentation in saturated systems is appreciably easier. to conduct. Generally, the colloid retention and mobility processes are considered to be similar in both systems. Among the key properties identified as controlling unsaturated colloid transport are: 1) degree of hydraulic unsaturation (Wan and Tokunaga 1997), 2) colloid size (McGraw 1996), 3) colloid surface properties (McGraw 1996, Wan and Wilson 1994a, Wan and Wilson 1994b), 4) flow rate (Goldenberg et al. 1989) and 5) pore size (Wan and Tokunaga 1997). Among these parameters, the ratio of the colloid size to the film thickness is frequently mentioned as a key governing factor (McGraw 1996, Choi and Corapcioglu 1997, Wan and Tokunaga 1997). A review of conceptual models governing unsaturated colloid transport is presented by Bennett et al. (1999).

Goldenberg et al. (1989) and then Wan and Wilson (1994a and 1994b) used micromodels to visualize colloid mobility in unsaturated systems. They showed that hydrophobic colloids preferentially sorbed to the air-water interface, and that they did not desorb from this interface. Wan and Wilson found that the degree of attachment was dependent on the surface charge, hydrophobilicty, and ionic strength. Goldenberg et al (1989) found that bubbles transport 20 to 50 times more hydrophobic colloids than the pure aqueous phase. The colloids at Yucca Mountain, are likely to be dominated by hydrophilic surfaces, whereas hydrophobic surfaces, which are commonly found in solids composed of large-aromatic organic compounds, are expected to be appreciably less common. They also observed that bubbles could pass through smaller pore throats by elongating their shape. These early unsaturated colloid transport experiments provided important insight into some possible transport mechanisms, but were limited insofar as they were limited to two-dimensions, the immobile phase was glass as opposed to mineral materials, the role of mobile and immobile waters, effect of colloid straining, entrapment into interstitial (dead-end) spaces, movement into small versus large pores, effects of volumetric water content, and change in porosity that could potentially affect colloid mobility.

Wan and Tokunaga (1997) recently proposed a film-straining theory which proposes that colloid transport can be retarded due to physical restictions imposed by thin water films in partially saturated porous media. They introduce the concepts of a "critical matric potential" at which thick film interconnections between pendular rings are broken and film straining begins to become effective. The ratio of colloid size to film thickness is critical in this model. The conceptual model was supported by laboratory column experimentation that were conducted by injecting colloid suspensions into the top of initially dry columns at a constant rate. Thus, these column experiments were not uniformly saturated spatially.

A new technique for studying colloid transport through unsaturated systems was recently evaluated in our laboratory (McGraw 1996). This technique is based on the Unsaturated Flow Apparatus (UFA). The UFA is a temperature-controlled centrifuge with a continuous flow rotor head. Colloid suspensions are introduced into two porous media columns that are rotated at high speeds by the centrifuge. Degree of saturation in the column is controlled by the centrifuge's rotational speed (centrifugal force) and the pump's flow rate. This instrument has successfully been used to measure hydraulic conductivity (ASTM D18.21 1996, Conca 1993, Nimmo et al. 1992), estimate recharge rates (Nimmo et al. 1994), study the movement of solutes in the vadose zone (Lindenmeier 1995, Kaplan et al. 1996), and measure the hydraulic properties of carbon tetrachloride (Shields 1995).

The centrifuge method experiments showed that colloid transport behavior in unsaturated systems could not have been predicted based on results from saturation flow experiments (McGraw 1996). For example, in a saturated system, colloid retention by a coarse-textured sand was not effected by colloid size (52 to 1900 nm). However, in a system of 6% volumetric water content, an increase in colloid size resulted in an exponential increase in colloid retention. The increase colloid retention at low moisture concentrations was directly related to the ratio between the water film thickness and colloid diameter. The most mobile colloids had diameters less than 60 nm. Additional experiments showed that small (20 to 280 nm) hydrophilic and hydrophobic colloids behave quite similarly in saturated systems but very differently in unsaturated systems (volumetric water content = 6%). In saturated systems, both types of colloids, irrespective of size, moved through the columns at approximately the same rate as water. In the unsaturated systems, the hydrophilic colloids tended to move through the sand at a rate similar to that of

water, whereas the hydrophobic colloids tended to move much slower than water, i.e., they were retarded. An important conclusion from this research is that some colloids, especially small hydrophilic ones, may be able to move through systems of extremely low moisture saturation.

Effect of Ionic Strength on Colloid Mobility Through Porous Media

Ionic strength is a measure of the concentration of salts in the aqueous phase (more precisely, it is the sum of the molar concentrations times its valence of each ionic species). It is anticipated that the ionic strength will be highest in the near field of the Yucca Mountain repository, where the contaminant plume may include the leachate of glass, cement, and other engineered barriers. The ionic strength of glass and cement leachate can vary greatly but commonly range between 1 to 0.01 (Mann 1998). As the plume travels further from the point source, it will take on the chemistry of the natural groundwater, which has an ionic strength of ~0.01.

Ionic strength affects colloid behavior in a number of ways. First it exerts a strong effect, along with the valance state of the dissolved ions, on the colloid surface charge. Increases in ionic strength tend to collapse the electrostatic double layer, which is an electrostatic halo around the colloid that provides repulsive forces to colloids or matix materials of similar charge. By collapsing the double layer, greater colloid-colloid or colloid-matrix interactions are expected. Greater colloid-colloid interaction results in the colloids aggregating, which in turn would cause the colloids to settle out of suspension more rapidly. Additionally, the aggregated colloids would have a larger effective colloid diameter, thereby increasing their propensity to be sieved as they move through porous media. Greater colloid-matrix interactions result in a greater likelihood of the matrix retaining the colloids. There are a number of mechanisms by which matrix materials can retain colloids (reviewed by Tien 1989). These retaining mechanisms can be broadly organized into electrostatic attraction and physical processes. Electrostatic attraction accounts for mobile colloid retention by oppositely charged particles. Physical attraction accounts for mobile colloid retention by straining, settling, and Brownian motion. Additional discussion of these retention processes will be presented below in the Theory Section.

Hypothesis and Objectives

Several researchers have conducted experiments to evaluate the effect of ionic strength on colloid mobility through saturated systems (Tobiason 1989, Elimelech and O'Melia 1990, Chang and Vigneswaran 1990, Elimelech 1992). Without exception, each study has shown that increases of ionic strength decreases colloid mobility. No one has evaluated the effect of ionic strength on colloid mobility through unsaturated systems. The **working hypotheses** for this study was that there is an interactive effect of ionic strength and degree of saturation on colloid mobility such that the effect of increasing ionic strength on colloid removal by the matrix is increases with degree of saturation. The **objective** of this study was to test this hypothesis under experimental conditions relevant to Yucca Mountain. For instance, the selection of groundwater chemistry (Kerrisk 1987), natural colloid concentration and size (Ogard 1987, Triay et al. 1994, Levy 1992), and matrix materials used in these experiments were based on conditions existing at Yucca Mountain. Additionally, the latex colloids used in these studies were selected to have similar surface potentials, hydrophilicity, concentration, and diameter as Yucca Mountain colloids. Initial experiments were designed to quantify the effect of ionic strength on colloid

settling and aggregation behavior. A second series of transport experiments evaluated the effect ionic strength and moisture saturation on colloid transport.

Theory

Colloid Aggregation and Colloid Deposition

Colloids can be removed from solution by the process of aggregation (colloid-colloid interaction) or deposition (colloid-solid media interaction) which is also termed filtration. Both processes involve particle-particle interactions, however the removal rates from solution are different. In this study, both processes were quantified as a function of ionic strength to help interpret the results of subsequent column studies. In particular, the intent of these studies was to provide information that could be used to determine whether the enhanced colloid removal observed at higher ionic strengths should be attributed to deposition or aggregation. It was not possible to differentiate between these processes based solely on the column breakthrough data.

Deposition describes colloid removal during transport through a sediment bed. The removal rate by deposition is a pseudo-first-order process, typically expressed as a function of distance, L, along the length of the porous medium,

$$\frac{dN}{dL} = -k_d N \tag{1}$$

where N is the number concentration of particles in suspension and k_d is the pseudo-first-order rate constant, which is proportional to physical and chemical properties of the system

$$k_d \propto \alpha_d \eta \tag{2}$$

(Stumm and Morgan, 1996). η is a dimensionless mass transport coefficient, and α_d is a dimensionless sticking coefficient that expresses the ratio of the rates at which particles attach, and approach, the collector (solid medium) (Stumm and Morgan, 1996).

The rate of removal by aggregation is a second-order process

$$\frac{dN}{dt} = -k_a N^2 \tag{3}$$

where t is time and k_a is a second-order rate constant, which is a function of physical and chemical properties of the system,

$$k_a = \alpha_a \beta \tag{4}$$

(Stumm and Morgan, 1996). Similar to α_d for deposition, the dimensionless sticking coefficient for aggregation, α_a, is conceptualized as a collision efficiency factor, or the fraction of collisions

that result in attachment (Stumm and Morgan, 1996). β is a mass transport coefficient that accounts for physical processes and is often evaluated theoretically (Stumm and Morgan 1996).

Three transport mechanisms can result in the aggregation of colloids from suspension: Brownian diffusion, laminar shear, and differential settling (O'Melia 1978). In a static settling test of uniform latex particles, laminar shear is absent because of the lack of advective water, and differential settling is absent because all the particles are of uniform size. The mass transport coefficient for colloid settling can then be simplified as resulting simply from Browning motion. The Brownian diffusion mechanism (β_{Bd}) is defined by O'Melia (1978) as:

$$\beta_{Bd} = \frac{4kT}{3\eta}. \tag{5}$$

Thus, **Equation 4** can be used to calculate the sticking coefficient, α_a, during a colloid settling test by first calculating β_{Bd} using **Equation 5** and then experimentally measuring the second-order rate constant, k_a.

DLVO Forces

The particle-particle interactions that result in colloid removal by deposition or aggregation are determined by a number of forces. These forces can be categorized as long-range forces and short-range forces. The long-range forces are also referred to as DLVO-forces, and they include the van der Waals attractive force and the double-layer repulsive or attractive force. The van der Waals force results from dipole interactions between molecules comprising the colloid and matrix particles. The magnitude of this force decreases significantly as a function of distance from the surface, generally diminishing to near zero beyond 1 nm from the surface (van Olphen 1977). The double-layer attractive or repulsive force results from the atmosphere of counter ions in the liquid phase surrounding charged particles. These counter ions electrostatically neutralize the charge of the particle. Particles of similar polarity will repulse, whereas particles of opposite polarity will attract.

Short-range repulsive forces, or non-DLVO forces, are generally confined to within a nanometer of the particle surface. They include steric, Born, and adsorbed hydrologic forces. Steric repulsive forces result from the nonideal (not flat) spatial arrangements of molecules on a surface. Born repulsive forces result from molecular interactions occurring from electron orbitals of approach particles overlapping. Adsorbed hydrologic repulsive forces result from the surfaces strongly adsorbing water molecules, thereby diminishing the ability of the particles to come into contact with each other. Short-range repulsion has been included in DLVO profiles in two ways: (1) by designation a minimum separation distance corresponding to the shear plane distance and the thickness of the layers of water of hydration between surfaces (Ryan and Gschwend 1994); and (2) calculations of the Born potential energy (Ruckenstein and Prieve 1976, Barouch et al. 1987). The application of either of these short-range potentials introduces a great deal of uncertainty to the calculations (Israelachvili 1992) given the complexity of the near-surface interactions and difficulty to measure the needed parameters. In practice these forces have been treated as fitting parameters (Barouch et al. 1987) or fixed at some assumed value (Ryan and Gschwend 1994).

Without inclusion of these uncertain estimates of short-term forces, DLVO theory is limited to describing only long-range forces applicable to greater than approximately 1 nm separation distance. This becomes especially important when attempting to predict remobilization, or desorptive, processes. One of the consequences of not including short-range forces is that DLVO theory must assume irreversible colloid deposition (because it assumes an infinitely deep primary minimum potential, as will be described in more detail below).

The repulsion potential, Φ_R (J), induced by moving two spherical particles of radii a_1 and a_2 (m) together from an initially large separation distance, h (m), may be approximated from the following (Shaw 1992):

$$\Phi_R = \frac{64\pi\varepsilon a_1 a_2 k^2 T^2 Y_1 Y_2}{(a_1 + a_2)e^2 z^2} \exp(-Kh) \tag{6}$$

where Y_i is the charge-dependent parameter for particle i as given by **Equation 7**, K is the Debye parameter as given by **Equation 8** (1/m), ε is the permittivity of the interparticle medium (C^2/Nm^2), T is the absolute temperature (K), e is the electron charge (1.6 x 10^{-19}C), z is the valence on the salt ions in solution (unitless), and k is Boltzmann's Constant (1.38 x 10^{-23} J/K). **Equation 6** assumes the Gouy-Chapman theory of a diffuse double layer and the Poisson-Boltzmann theory of the distribution of electrical potential within the diffuse layer.

The charge-dependent parameter, Y, used in **Equation 6** was calculated as follows:

$$Y_i = \tanh\left(\frac{ze\psi_i}{4kT}\right) \tag{7}$$

where ψ_i is the surface potential of particle i (V). **Equation 6** is valid when ψ_1 is approximately equal to ψ_2 and they are <60 mV. The Debye parameter, K, which is related to the double-layer thickness, was calculated using **Equation 8**:

$$K = \left(\frac{2e^2 N_A c z^2}{\varepsilon kT}\right)^{0.5} \tag{8}$$

where N_A is Avogadro's number (6.02 x 10^{23} molecules/mole), and c is the ionic strength of a z:z electrolyte (an electolyte consisting of a cation with a valence of z and an anion with a valence of z). **Equation 6** is based on the assumption that Ka_i >5.

Van der Waals attractive forces, Φ_A, are created by the dipole interactions between atoms and molecules comprising the particles. They can be estimated as follows (Hiemenz and Rajagopalan 1997):

$$\Phi_A = -\frac{A}{6}\left[\frac{2a_1a_2}{h^2 + 2a_1h + 2a_2h} + \frac{2a_1a_2}{h^2 + 2a_1h + 2a_2h + 4a_1a_2} + \ln\left(\frac{h^2 + 2a_1h + 2a_2h}{h^2 + 2a_1h + 2a_2h + 4a_1a_2}\right)\right] \tag{9}$$

where A is the Hamaker constant (J). As **Equation 9** shows, the attractive force is not affected by ionic strength. Finally, the total interparticle potential, Φ_T is the sum of the attractive and repulsive potentials:

$$\Phi_T = \Phi_A + \Phi_R. \tag{10}$$

Based on DLVO theory, the propensity of a colloid to remain dispersed, coagulate, or slowly flocculate from suspension can be determined from potential diagrams, which display the total potential (**Equation 10**) as a function of separation distance (h). Examples of potential diagrams illustrating these three colloid conditions are presented in **Figure 1-1**. The convention for this theory is that attractive forces have negative signs and repulsive forces have positive signs. The net interparticle potentials in **Figure 1-1**, as well as through out the text, were normalize by the thermal energy (kT) of the particle. This dimensionless parameter (J/[J/K·K]) normalizes the data to the net forces responsible for Brownian motion, which is the result of thermally induced molecular vibrational forces. The negative of $d\Phi/dh$ represents the force encountered by the approaching particle. When $d\Phi/dh$ is negative, the force encountered is repulsive in nature.

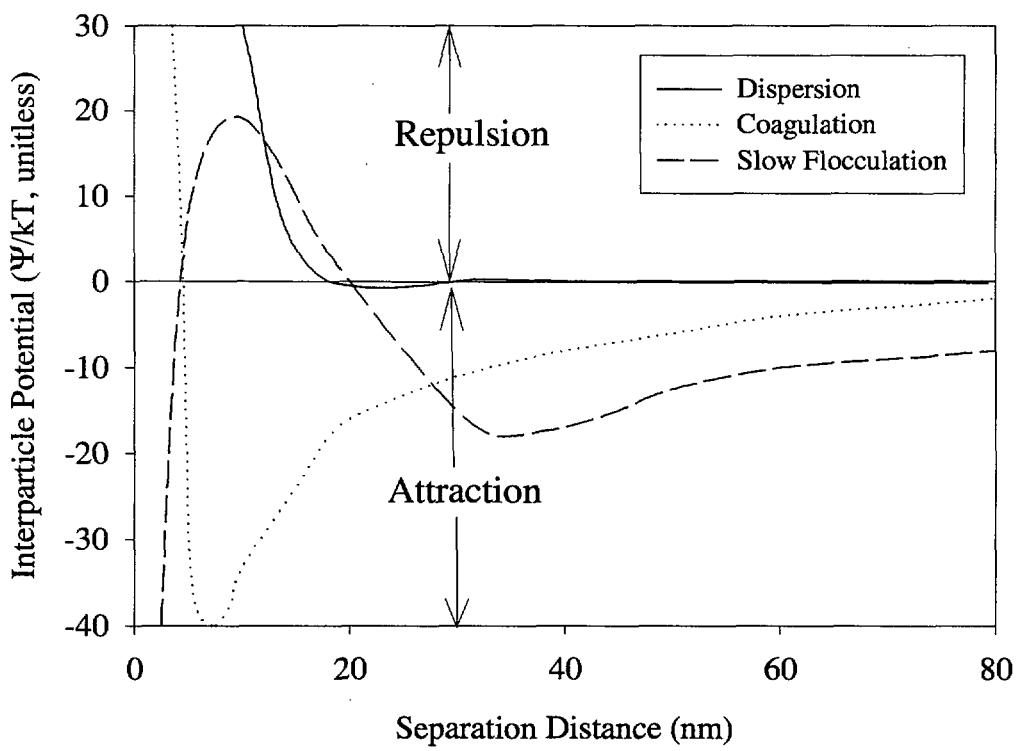

Figure 1-1
Example of Interparticle Potential Plots Displaying Dispersion, Coagulation, and Slow Flocculation Based on DLVO Calculations

As the separation distance increases, the interparticle potentials approach zero, i.e., the solid phase has no electrostatic influence on chemical composition of the water (**Figure 1-1**). The maximum potential, which occurs generally at separation distances of <20 nm, is termed an energy barrier. This is because particles of similar polarity experience a repulsive force as they

approach each other, and only those with greater energy than the maximum potential energy can continue to approach. Once the particles pass the energy maximum, they approach the primary minimum. Particles existing in the primary minimum tend to aggregate. Particles can be brought out of this energy minimum by a number of ways, including increasing temperature or introducing shear force. Ionic strength strongly affects the height of the energy barrier, as will be shown below. It exerts its affect on the energy barrier by influencing repulsive, and not attractive, forces. To ensure a reasonably stability of a suspension, the energy barrier height should be greater than about 15 kT for a dilute solution of colloids (van Olphen 1977). For a more concentrated suspension, the energy barrier should be greater than 25 kT to produce a stable suspension (van Olphen 1977). Thus, a potential diagram in which the energy barrier is >15 kT would be expected to be dispersed and the colloids would not contain sufficient energy to overcome the primary maximum (**Figure 1-1**). A potential diagram in which the interparticle potentials are always ≤0 is indicative of coagulation and in the context of colloids moving through a column would suggest a strong likelihood of colloid removal. A condition intermediate between complete dispersion and complete coagulation is slow flocculation. Slow flocculation is expected when the interparticle potential has a secondary minimum of <15 and only a moderately high-energy barrier of <20. Additional discussions of the interpretation of energy potential diagrams as they relate to energy minimums, activation energy, and energy minimum "traps" is offered by Hiemenz and Rajagopalan (1997) and van Olphen (1977).

Critical Coagulation Concentration (CCC)

DLVO theory predicts that there is a critical ionic strength of indifferent electrolytes above which, colloids will coagulate; this is referred to as the critical coagulation concentration (CCC). Numerous experiments have substantiated that there is in fact a critical concentration, beyond which suspended colloid concentrations decrease sharply. However, DLVO theory does not provide a quantitative estimate of experimentally derived CCC values (Hiemenz and Rajagopalan 1997). However, the theory does predict important trends that have been repeatedly observed experimentally, including:

1. The higher the potential at the surface of a particle, the larger the repulsion between the particles will be.

2. It is the valence of the ion of the opposite charge to the colloid that has the principal effect on colloid stability. The CCC value for a particular electrolyte is essentially determined by the valence of the counter-ion regardless of the nature of the ion with the same charge as the surface. This is referred to as the Schulze-Hardy rule.

In nature the CCC is primarily controlled by three aqueous properties and one solid-phase property. The primary aqueous properties are 1) pH, 2) the valence of the counterion in solution (Schulze-Hardy rule), and 3) the solution ionic strength. The primary solid phase property controlling CCC is the surface charge of the particle (particle morphology is also important for some minerals, such as illite).

Based on an exhaustive review of literature CCC values, Summer (1993) showed that for Na systems, the CCC for smectite and mica was less than ~0.01 M. For Ca systems, the CCC for the same minerals was less than ~0.005 M. He did not provide CCC values for silicates, iron

oxyhydroxides, and zeolites, the other natural colloids, found at Yucca Mountain.. The CCC of silicates and iron oxyhdroxides are likely lower than those listed for smectite and mica because the surface charge of the former minerals are lower than the latter minerals. Silicates, the dominant colloid found in Yucca Mountain water, has a low surface charge (Kaplan et al. 1993) and therefore would be expected to have a lower CCC than the smecite and mica values offered by Sumner (1993). Iron oxyhydroxides have a pH dependent charge, whereby the surface charge becomes increasingly more negative above the zero-point-of-charge (ZPC), which is around pH 9 (Stumm and Morgan 1996), and increasingly more positively charged as the pH decreases below the ZPC. Thus, under typical pH conditions of 6.5 to 9.4 , the iron oxyhydroxides may be expected to have either no charge or a slight positive charge. Considering that the most dilute water that the waste will come into contact with has an ionic strength of ~0.01 (or ~0.01 M), and that this water will contain both sodium and calcium, it appears that the aqueous system will always have an ionic strength greater than expected CCC values. (It should be noted, that dilution as low as that of rain water may be possible under episodic rain events; however, such conditions are not likely or widespread, considering that once the rain water comes into contact with the solid phase, salts from the solid phase will enter the aqueous phase.) The point of this discussion is to illustrate that even if radionuclide-bearing colloids exist in the system (and their existance is highly likely), it does not seem likely that they will remain in suspension sufficiently long to move great distances.

2
EXPERIMENTAL RESULTS

Materials

A 90% quartz sand (Accusand®, Unimin Corp.) was sieved between 20 and 30 mesh (590-850 μm), washed with de-ionized water, and air-dried prior to use. A geologic sample of Yucca Mountain was supplied by Chris Lewis of the Sample Management Facility of the Yucca Mountain Project. The sample was collected from an outcropping of the Topopah Spring member of the Paintbrush Tuff (likely of the Tptp mn lithophysal). The rock was crushed and dry sieved between 40 and 60 mesh (250-425μm) to a particle size range of 0.25 - 0.40 mm. SEM, EDX, and XRD analyses of the crushed tuff material and SEM of the quartz sand were conducted. The purpose of the SEM analyses was to quantify the size of the particles and to compare their morphologies. The average width and length of the sand particles was 710 ± 106 and 723 ± 198 μm (n = 20). The average width and length of the crushed Yucca Mountain tuff material was somewhat smaller, 634 ± 134 and 514 ± 117 μm (n = 20). The primary morphological difference between the two matrix types was that the quartz had very rounded edges, whereas the tuff had a very coarse surface with many sharp edges (Figure 2.1). The importance of these morphological observations is that the crushed tuff material appeared to clearly have more sites for colloid retention.

X-ray diffraction analysis identified quartz as the dominant mineral in the sand (data not presented). Trace concentrations (<5%) of mica were also detected. The mica could also be seen with the naked eye. Given the dark color of the mica, it was likely biotite. The crushed tuff contained a substantial amount of silicates, feldspar, and an amorphous component, likely glass (Figure 2.2). Additionally, there were trace concentrations of a phyllosilicate, likely mica or vermiculite.

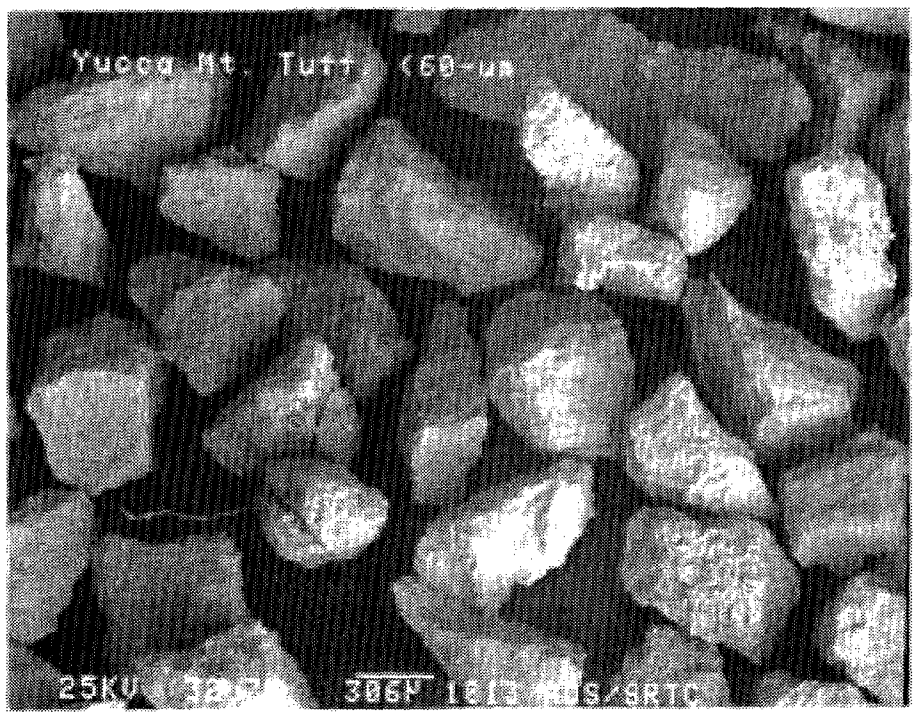

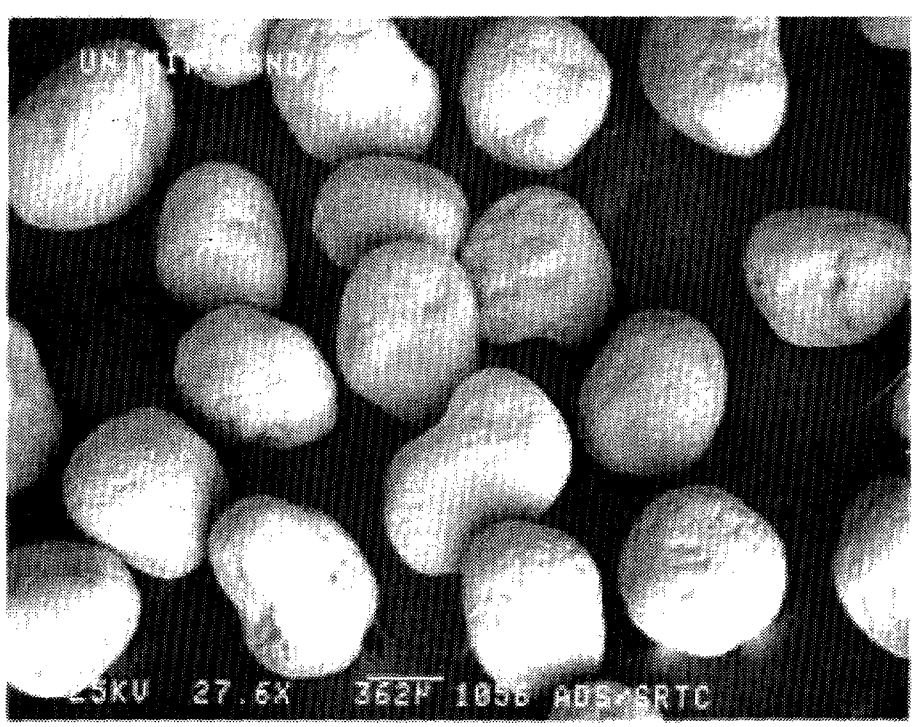

Figure 2-1
Scanning electron micrographs of the crushed tuff (top) and quartz (bottom) used as matrix material in this study. The quartz was slightly larger and appreciably smoother than the crushed tuff.

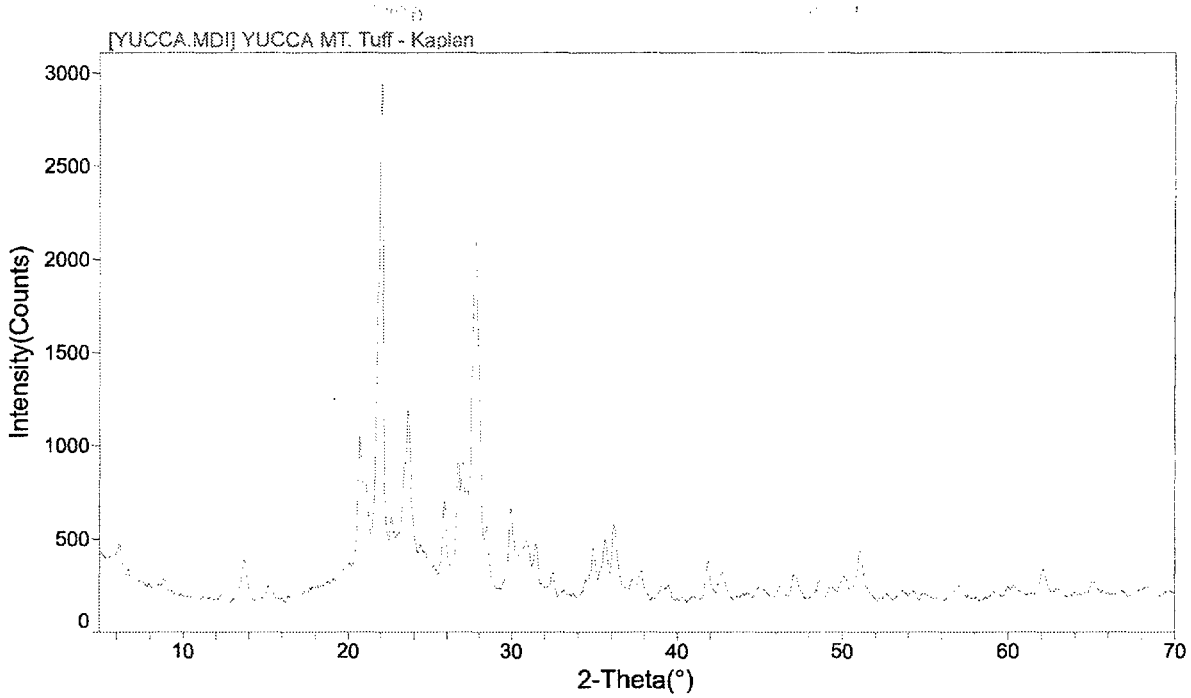

Figure 2-2
X-ray diffraction scan of the crushed tuff material (Topopah Spring) used in this study

Columns were hand-packed with these materials and saturated with aqueous solution prior to initiating colloid transport. The standard formulation of synthetic J-13 groundwater is 0.368mM Na_2CO_3 and 10.6mM $NaHCO_3$, pH=7.8. Due to difficulty in maintaining this pH, and in an effort to maintain a consistent ionic strength (I), the baseline solution (1x) was prepared as above, without pH adjustment. Varying dilutions of this solution were prepared for colloid settling and coagulation experiments: 0x (deionized water), 0.1x, 0.5x, 0.75x, 1x, 2.5x, 5x, 7.5x, and 10x. The ionic strength and initial pH of the solutions used in transport experiments at ambient laboratory conditions are summarized in Table 2-1. De-ionized water that was passed through a Milli-Q system (Millipore Corp., Bedford, MA) is referred to as "0x" and represents the practical lower limit of I. The initial pH of the solutions used in transport experiments at ambient laboratory conditions.

Table 2-1
Ionic Strength and Average pH of Aqueous Solutions Used in Transport Experiments

Solution	10x J-13	1x J-13	0.1x J-13	0x J-13
Ionic Strength	1.16×10^{-1}	1.16×10^{-2}	1.16×10^{-3}	-
average pH	8.8	8.7	8.5	7.6
standard deviation	0.3	0.05	0.2	0.1
n	3	4	3	4

Note that due to the buffering action of the sodium carbonate/bicarbonate solution, the average pH of the synthetic J-13 solutions is 8.6 with a standard deviation of 0.2. The pH of the 0x, or "pure" water solution is 1 unit lower, indicating an order of magnitude difference in hydrogen ion activity. Possible effects of pH on colloid transport are addressed below and with the results.

Carboxyl-modified polystyrene latex (CML) microspheres, 0.030 μm i.d. were obtained with fluorescent crimson dye (Batch 2-FC-30.6312,1, Interfacial Dynamics Corp., Portland OR). According to the manufacturer, the colloids have a high density of carboxyl groups on the surface, and throughout the shell, with a relatively low density of sulfate groups at the surface. The pK_a of the CML particles is ~ 9-10 and the colloids are considered to be hydrophilic at high pH or ionic strength. The pK_a value of 9-10 indicates that surface charge depends on pH. At pH values of 1.5 units less than the pK_a (i.e., 7.5-8.5), the protons of the carboxylic acid functional groups will be associated, and the surface charge will be predominately neutral. At pH values in the range of the pKa, approximately half of the protons of the carboxylic acid functional groups will be associated, while half will be dissociated, or released to solution. At pH values greater than the pK_a, an increasing fraction of the carboxylic acid functional groups will be dis-associated, and the surface charge will be more negative. At the lower pH value of the 0x solution (7.6), the surface will be more neutral, and possibly more hydrophobic. Decreased colloid mobility or increased deposition on the sediment would be evidence of greater hydrophobicity.

The concentration of colloids in aqueous solutions was determined using using fluorescence spectroscopy (Model L550B Luminescent Spectrophotometer, Perkin-Elmer Corp., Norwalk, CT). The excitation and emission wavelengths, λ, were 619 and 645 nm, respectively. Colloid concentrations were based on a 5 point linear calibration curve, bracketing the initial concentration, c_o, used in transport experiments and ranged from 4.35 to 4.77 mg/L. Glassware was acid washed (10% nitric). Bromide (Br^-, c_o = 5000 to 6000 mg/L) and pentafluorobenzoic acid (PFBA, c_o = 100 mg/L) were used as conservative tracers to monitor hydrodynamic conditions in separate experiments. Bromide was used initially; solution concentrations were determined by ion selective electrode (Orion Research Inc., Beverly MA). PFBA was later adopted due to increased analytical precision and was analyzed directly in the column effluent by online UV detection at 254 nm (Model 119, Gilson, Middletown, WI).

Particle Characterization

Average particle size was determined by measuring and averaging approximately 20 SEM images of colloid and matrix particles. Electrophoretic mobility was measured using a Coulter Delsa 440 (Coulter Corporation, Miami, FL). Suspensions of ~1 mg L^{-1} 280-nm latex particles were prepared in varying concentrations of simulated J-13 water.

To provide a measure of the surface charge of the matrix, the sand was ground to clay-size particles (<2 μm) and then diluted in synthetic J-13 water to a final concentration of ~ 1 mg L^{-1}. Triplicate multiangle measurements were made of mildly sonicated (20 s in a 14 cm x 14 cm x 24-cm water bath at 150 W) samples at four angles (9°, 17°, 26°, and 35°). An NTIS traceable standard was carried through the analysis (the EMPSL7 –3.93 ± 0.36 μm·cm/V·s standard measured –3.78 ± 0.05 μm·cm/V·s). The resulting data were analyzed by the Marquadt

Minimization procedure, an iterative least-squares procedure (Cummins and Staples 1987). Electrophoretic mobility was converted to zeta potential using Smoluchowski's equation (Heimenz and Rajagopalan 1997) and zeta potential was used as an approximation of the surface potential, Ψ.

The ionic strength of the various solutions used in the electrophoretic mobility measures, except the 0x solution, were calculated using MINTEQA2 (Allison et al. 1983). The ionic strength of the 0x solution was estimated by first measuring the electrical conductivity (*EC*) and then converting that value to ionic strength (*I*) using the empirical relation: $I = 0.013EC$, where I is in units of mol L^{-1} and *EC* is in units of $(\Omega\ m)^{-1}$ (Griffin and Jurinak 1973).

Gravitational Settling and Critical Coagulation Concentration

Colloid settling experiments and determination of the critical coagulation concentration (CCC) were conducted using 4 mg L^{-1} suspensions of the fluorescent 280-nm colloids prepared in various concentrations of synthetic J-13 water (10x, 5x, 3x, 1x, 0.7x, 0.3x, 0.1x, and 0x [deionized water]). Sonicated suspensions were placed directly in 5-mL cuvettes and fluorescence was measured periodically during a 445-min settling period. Based on Stoke's Law, the distance that a singlet colloid would settle during this settling period was insignificant, 6.7e-5 m (for the following conditions: temperature = 25 °, water density = 997 kg m^{-3}, particle density = 1050 kg m^{-3}, viscosity = 9.11e-4 kg m^{-1} s^{-1}, time = 26,640 s, particle diameter = 290e-9 m). This distance represents <0.1% of the total height of the 4.5-cm tall cuvettes. Thus, changes in fluorescence can be attributed to reduction in colloid concentration, which in turn may be attributed to aggregates, and not singlets, settling out of suspension. So it was assumed that any decrease in particle concentration was attributed to particles settling out of suspension. To use **Equations 3** through **5**, it was further assumed that only doublets were formed.

The settling experiments permitted direct measurement of the CCC. The CCC is an empirical construct that provides the minimum ionic strength of a salt solution required to induce coagulation. DLVO theory accurately predicts trends but not the absolute values of CCC (van Olphen 1977). Identification of the CCC in this study was based on the concentration of the colloids in suspension at the end of the settling experiment, 445 min. The CCC was the minimum salt concentration to induce a drastic decrease in suspended colloid concentrations. It was determined by evaluating the fluorescence data, although it was possible to identify the CCC by observing the colloid suspensions with the naked eye.

Transport Method for Saturated Columns

Miscible displacement experiments were conducted using standard techniques (Zhong et al., 1986; Gamerdinger et al., 1991; 1994) and were designed to simulate expected Yucca Mountain conditions (Table 2-2). Glass columns, 2.5 cm i.d. (Kontes, Vineland, NJ), were equipped with Teflon bed supports, mesh, and tubing to avoid interaction of the colloids. An infusion pump (AVI® Micro 210, AVI, Inc., St. Paul, MN) was used to saturate the columns, maintain steady-state flow, and to deliver colloid, tracer, and tracer-free solutions. With the exception of the compressible bladder, the pump tubing was replaced with teflon tubing; solutions were delivered from glass bottles. Due to the limited supply of tuff, experiments were executed consecutively

on each column. Potential effects on colloid deposition and hydrodynamics were evaluated by repeating the initial conservative tracer and colloid transport experiments after completion of the other experiments. The length, L, and bulk density, ρ_b, of the sand (S) and tuff (T) columns were 15.99 cm, 5.60 cm, 1.79 g cm^{-3}, and 1.261 g cm^{-3}, respectively. The volumetric water content, (cm^3 cm^{-3}) was determined by mass; the average pore water velocity, v (cm hr^{-1}) was measured directly. Tracer and colloid solutions were applied in separate experiments as step inputs to the columns where the pulse size, t_o, is defined as the length of the step input, expressed as the number of column pore volumes. A pore volume (PV) is defined as the volume of water retained within the pore space of the sediment bed. Effluent was collected by automated fraction collector (Br^- and colloids) or analyzed directly (PFBA). The pH of effluent samples was monitored as an indicator of geochemical stability during selected experiments.

Table 2-2
Experimental conditions used in saturated and unsaturated colloid transport studies

Parameter	Description	Comment
Colloid Conc.	4 mg/L	Kingston and Whitbeck (1991) reports colloid concentration between 0.28 to 25 mg/L in 24 springs and wells at NTS; 21 colloid concentrations ranged from 0.28 to 1.35 mg/L
Column Dimensions	Saturated: 5.60 to 15.99 cm length; 2.5 cm diameter; 27.48 to 78.45 cm^3 Unsaturated: 6.00-cm; 2.25 diameter; 95.43 cm^3	Maintained a colloid diameter to column width ratio much greater than 40 (Relyea 1982), the minimum ratio below which edge effects will affect colloid diffusion and therefore colloid transport.
Immobile Phase	Sieved Topopah Spring tuff ground and sieved to 250-425μm; Quartz sand sieved to 590-850 μm	Two immobile phases will be present, fractured and porous media. Porous media was selected for this study because of its experimental simplicity.
Colloid Properties	Fluorescent hydrophilic 280-nm latex microspheres	YM colloids are expected to be inorganic and little or no organic component. Based on mineralogical considerations, colloids generated from the tuff or formed from glass dissolution will have predominantly hydrophilic properties. Triay et al (1996) reported that 25%, 40%, and 35% of the total colloid mass in J-13 water existed in the 100 to 200 nm, 200 to 500 nm, and 500 to 1000 nm filter size range; hence 280-nm is within the size range likely to exist. A colloid diameter of 200-nm is commonly used by YM modelers (Stockman 1998; McGraw et al. 1998).
Aqueous Phase	0x, 0.1x, 1x, and 10x the chemical composition of simulated J-13 groundwater: 0.368mM Na_2CO_3 and 10.6mM $NaHCO_3$ (pH=7.8).	This recipe of a simplified J-13 groundwater is used extensively (e.g., see numerous examples in Triay et al [1994]).
% saturation	~15, ~60, and 100%	
Flow velocity	Saturated: 12 to 38 cm hr^{-1}; Unsaturated: 15 to 24 cm hr^{-1}	Flow rate is expected to vary greatly depending on saturation, and whether porous or fracture media are involved. As a point of reference, Thompson (1989) used 2 cm hr^{-1} in saturated crushed tuff column experiments.

Transport Method for Unsaturated Columns

The unsaturated column system system consists of two volumetric infusion pumps (AVI 210A, 3M, St. Paul, Minnesota) and an "unsaturated flow apparatus" (L8-UFA®, Beckman Coulter, Inc., Fullerton, CA). The L8-UFA® includes a rotating seal, rotor, and what we term the "column assembly". The column assembly includes all of the fittings for containing a sediment sample, attaching the effluent collection cup, and connecting them to the rotor and rotating seal. The rotating seal is at the center of the rotor and is the conduit through which fluid is delivered from the pump to the columns, by two independent flow paths (Conca and Wright, 1992). The paths are termed "central" and "annular" designated as "c" and "a", respectively. These terms refer to the flow path within the rotating seal.

Columns were saturated with a minimum of 10 pore volumes of aqueous solution prior to connecting, and establishing unsaturated steady-state flow with the UFA®. The rate of fluid delivery to the column is fixed, and controlled with the pump. During operation of the centrifuge method, the average volumetric water content is influenced by a combination of the centrifugal force (controlled by the rotation speed of the centrifuge) and the fluid flux. Centrifugation forces water from the column, which is replaced by fluid delivery via the pump. Miscible displacement or unsaturated transport experiments were initiated when the columns reached a steady-state average water content.

Experiments were conducted in a manner similar to that used for saturated column experiments (above). A step input of the aqueous solution containing the conservative tracer or colloids was applied. The column was then flushed (at the same volumetric water content) with tracer-free aqueous solution. When switching influent solutions, columns were disconnected from the rotor, the tubing was drained, and refilled with the new solution. Column effluent was collected and analyzed to determine the flux-averaged effluent concentration. The average water content was determined by mass at each sampling point and the cumulative effluent volume was determined from the mass of the effluent samples. Dimensionless breakthrough curves (BTCs) were determined by plotting the normalized concentration versus the cumulative volume, expressed as pore volumes. BTCs were evaluated with appropriate mathematical models to determine transport parameters.

3
RESULTS

Particle Characterization

The influence of ionic strength on the zeta potential of the 280-nm latex particles is presented in **Figure 3-1.** As expected, increases in ionic strength caused a near linear decrease in zeta potentials. It is important to note that the zeta potentials of these latex particles are well within the range of zeta potenials measured for natural colloids. Colloids collected from the Savannah River Site, dominated with goethite, kaolinite, quartz and hydroxy-interlayered vermiculite, had an average zeta potential of –42 mV (Kaplan et al. 1995). Zeta potential values for dispersible clays collected from surface or near surface sediment collected from the New Jersey Coastal Plain were about –25 mV (pH 7 to 10) (Ryan and Gschwend 1994); from the South Carolina Coastal Plain were –41 to –18 mV (Kaplan et al. 1993). Thus, the surface potential of the latex particles used in these experiments are within the range that may exist at Yucca Mountain.

DLVO calculations (**Equations 6, 9, and 10**) were conducted using these values as estimates of the colloid surface potential. Additional input parameters for the DLVO calculations are presented in **Table 3-1.** Potential plots (total interparticle potential as a function of separation distance, e.g., **Figure 1-1**) were created simulating the approach of a 280-nm, latex particle to a sand-matrix particle in 0x, 0.1x, 0.5x, 0.75x, 1x, 2.5x, 5x, 7.5x, and 10x synthetic J-13 groundwater. Zeta potential values based on electrophoretic mobility measurements were assumed to estimate colloid surface charge. Electrophoretic mobility measurements were not made for the 0% and 10% J-13 groundwater concentrations due to instrumental limitations. Surface potentials for colloids in these solutions were estimated using **Figure 3-1.**

Interparticle potential diagrams show that as the ionic strength increased, the primary energy barrier decreased. Using 15 kT as the minimum energy barrier necessary for a dispersed system (van Olphen 1977), we would expect that no colloids would pass through sand treated with >~58 mol m^{-3} (5x J-13). Colloids would be retained to a progressively smaller degree as the ionic strength decreased below 58 mol m^{-3} (5x J-13 water). Relating these results to Yucca Mountain, the ionic strength of J-13 is approximately 11.6; therefore under far field conditions, DLVO theory would predict some degree of colloid stability in the far field. This result is contrary to previous discussion of literature experimental CCC values for minerals that indicated that J-13 water likely had a higher ionic strength than the CCC (see the Critical Coagulation Concentration section in the Introduction).

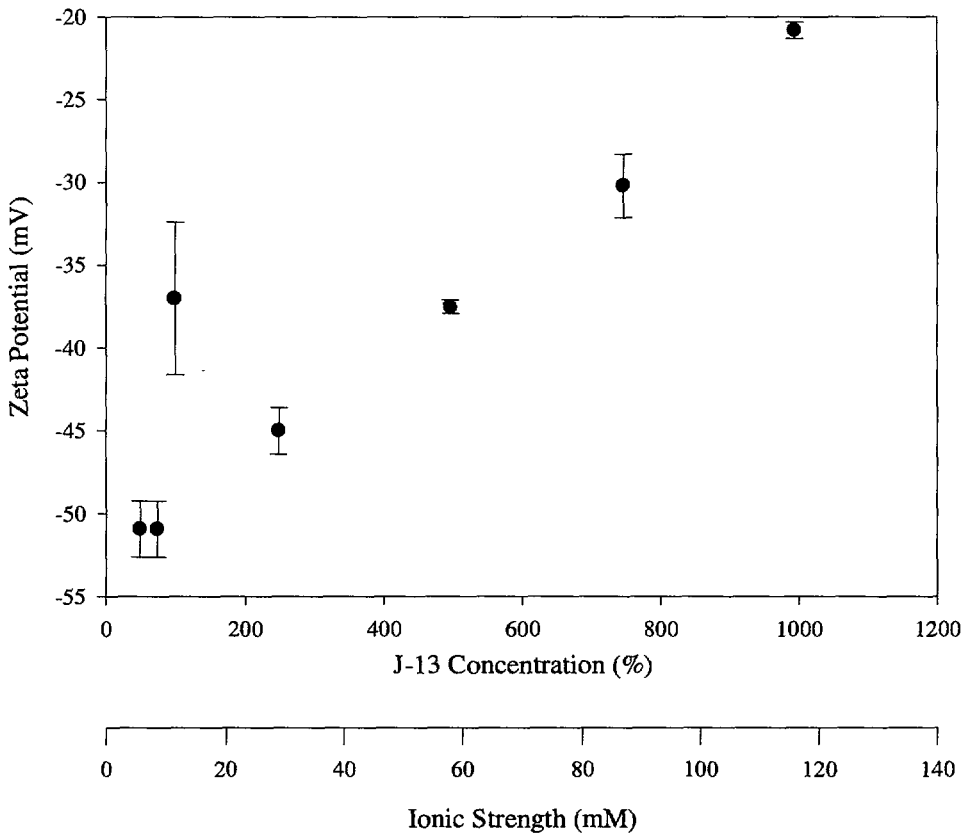

Figure 3-1
Zeta Potential of 280-nm Latex Particles as a Function of Synthetic J-13 Groundwater Concentration and Ionic Strength (Vertical Lines Represent Standard Deviation of 12 Values)

Table 3-1
Input Values Used in DLVO Calculations

Symbol	Description	Value	Units	Comments[a]
c-10x	Ionic Strength of 10x J-13	116	mol/m^3	From aqueous chemical speciation calculations made with MINTEQA2 (1)
c-7.5x	Ionic Strength of 7.5x J-13	87	mol/m^3	(See comment for *c*-10x)
c-5x	Ionic Strength of 5x J-13	58	mol/m^3	(See comment for *c*-10x)
c-2.5x	Ionic Strength of 2.5x J-13	29	mol/m^3	(See comment for *c*-10x)
c-1x	Ionic Strength of 1x J-13	11.6	mol/m^3	(See comment for *c*-10x)
c-0.75x	Ionic Strength of 0.75x J-13	8.7	mol/m^3	(See comment for *c*-10x)
c-0.x5x	Ionic Strength of 0.50x J-13	5.8	mol/m^3	(See comment for *c*-10x)
c-0.1x	Ionic Strength of 0.10x J-13	1.16	mol/m^3	(See comment for *c*-10x)
c-0x	Ionic Strength of 0x J-13	7e-4	mol/m^3	Based on electrical conductivity measurement
Ψ-10x	Colloid potential – 10x J-13	-0.0208	V	Measured
Ψ-7.5x	Colloid potential – 7.5x J-13	-0.0302	V	Measured
Ψ-5x	Colloid potential – 5x J-13	-0.0375	V	Measured
Ψ-2.5x	Colloid potential – 2.5x J-13	-0.0450	V	Measured
Ψ-1x	Colloid potential – 1x J-13	-0.0370	V	Measured
Ψ-0.75x	Colloid potential – 0.75x J-13	-0.0509	V	Measured
Ψ-0.5x	Colloid potential – 0.5x J-13	-0.059	V	Measured
Ψ-0.1x	Colloid potential – 0.1x J-13	-0.0525	V	Estimated from Figure 3-1.
Ψ-0	Colloid potential – 0x J-13	-0.0530	V	Estimated from Figure 3-1.
A-colloid	Hamaker constant-colloid	1.20e-20	J	(2)
A-matrix	Hamaker constant – sand matrix	1.24e-20	J	Average of three values (J x 10^{-20}): 1.3 (3), 1.6 (4), 0.83 (2).
Ψ-matrix	Sand matrix surface potential	-0.023	V	Based on electrophoretic mobility measurements of <2-μm sand particles. Assumed zeta potential = surface potential
a-colloid	Colloid radius	1.4e-7	m	Measured using SEM images
a-matrix	Matrix radius	3.25e-4	m	Measured using SEM images
z	Ion charge	1	unitless	
e	Electron charge	1.60e-19	C	
k	Boltzmann's constant	1.38e-23	J/K	
T	Temperature	298	K	
ε	Permittivity	6.73e-10	C^2/Jm	
N	Avogadro's number	6.02e23	m^{-3}	

[a] References: 1 = Allison et al. (1991); 2 = Israelachvili (1991); 3 = Anandarajah and Chen, 1995), 4 = Ackler et al. (1996).

The primary energy barrier values of these simulated systems are presented in **Figure 3-2**. The primary energy barrier values were plotted as a function of the square root of the ionic strength to reflect the approximate relation between ionic strength (c) and repulsive force (Φ_R) reflected in **Equations 6 and 8**. The regression coefficient of this relation (shown in **Figure 3-3**) was significant ($P \leq 0.01$). For future discussion, it is important to note that the relationship between these two variables are near linear.

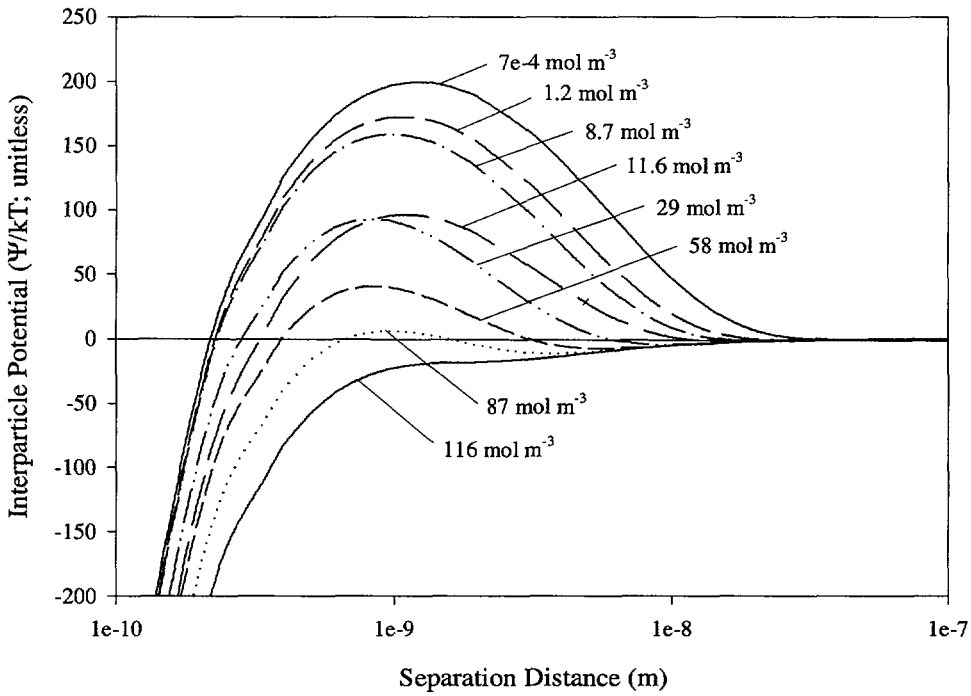

Figure 3-2
Interpartical Potential as a Function of Separation Distance and Ionic Strength (Based on Equations 6 through 10 and Input Values in Table 3-1)

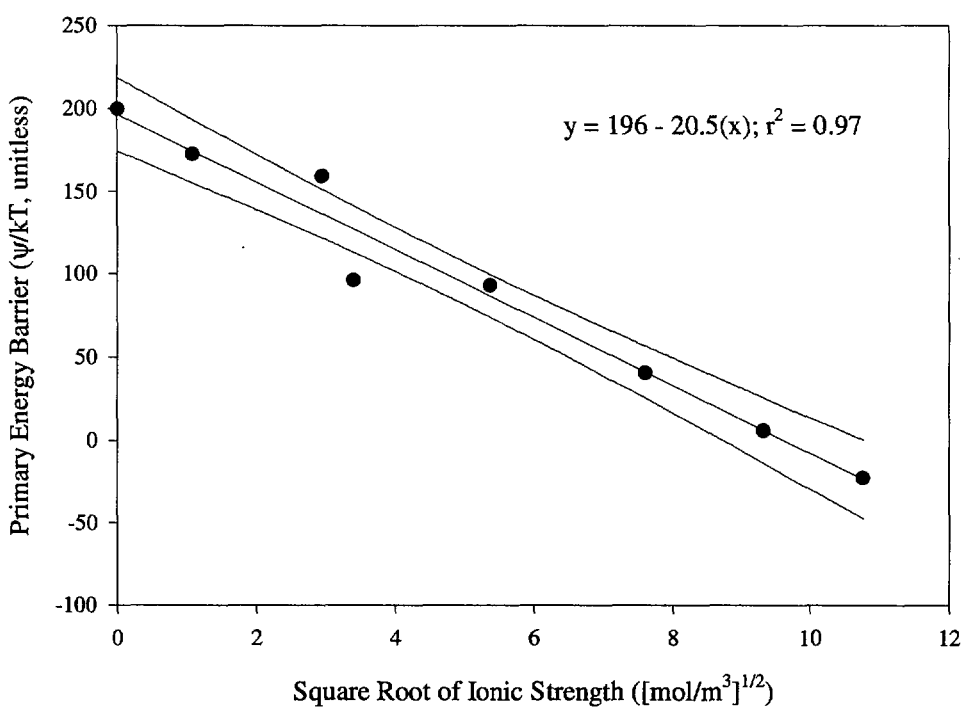

Figure 3-3
Primary Energy Barrier as a Function of Ionic Strength. Regression and 2σ Confidence Limits of the Regression Analysis are Presented

Gravitational Settling and Critical Coagulation Concentration

Gravitational settling experiments were conducted with the same fluorescent, 280-nm latex colloids used in the column experiments. Decreases in fluorescence were assumed to be due to particles aggregating together, thereby decreasing their buoyancy and increasing their settling rate. Calculations, presented in the Material and Methods section, indicated that singlet colloid settling due to Stokes Law (a measure of gravitational settling of spheres) would move <0.1% of the cuvette's total height. This suggests that gravatational settling of the singlet sphere is likely not responsible for the observed changes in fluorescence.

The critical coagulation concentration, CCC, for the 280-nm latex colloids was measured from the settling experiments with varied concentration of the synthetic J-13 water (sodium carbonate/sodium bicarbonate system). The CCC was 58 $mol_c\ m^{-3}$ (58 mol m^{-3} of the sodium carbonate/bicarbonate solution or 5x J-13 groundwater). Ionic strengths equal to or greater than the CCC would be expected to induce coagulation, whereas concentrations less than the CCC would be expected to induce either slow flocculation or dispersion **(Figure 1-1)**. The CCC did not change after 120 min of settling. Prior to 120 min, ionic strength treatment effects were not evident.

Equation 3 was used to calculate the second-order rate constant at each ionic strength. The second-order rate law fit well to the data; regression coefficients (R^2) of the fitted data to the measured values ranged from 0.882 to 0.996, all significant at $P \leq 0.01$ (data not presented). The second-order rate constants and the mass transport coefficients **(Equation 5)** were then used in **Equation 4** to calculate the sticking coefficient. This data is presented in **Figure 3-4.** At low ionic strengths, ≤58 mol m^{-3}, second-order rate constants increased with increased ionic strength. Above 58 mol m^{-3}, the second-order rate constant does not change appreciably. The lack of trend at the higher ionic strengths may be attributed to the ionic strength of the suspensions exceeding the CCC.

Transport Experiments in Saturated Columns

Results of transport experiments are expressed as breakthrough curves (BTCs), which depict the dimensionless effluent concentration (c/c_o) as a function of cumulative pore volumes eluted. The percent recovery of the analyte in the effluent was based on the area under the BTC compared with the measured step input. The fraction of colloids that was not recovered in the effluent was considered to be deposited on the porous media. The retardation factor, R, is defined as the average velocity of water relative to that of the solute or colloid. R values were determined from the area above the BTC (Nkedi-Kizza et al., 1987) for all but experiments S-9 and T-5. The lack of a clear plateau for colloid transport in the 10X synthetic J-13 solution precluded this analysis in experiments S-9 and T-5.

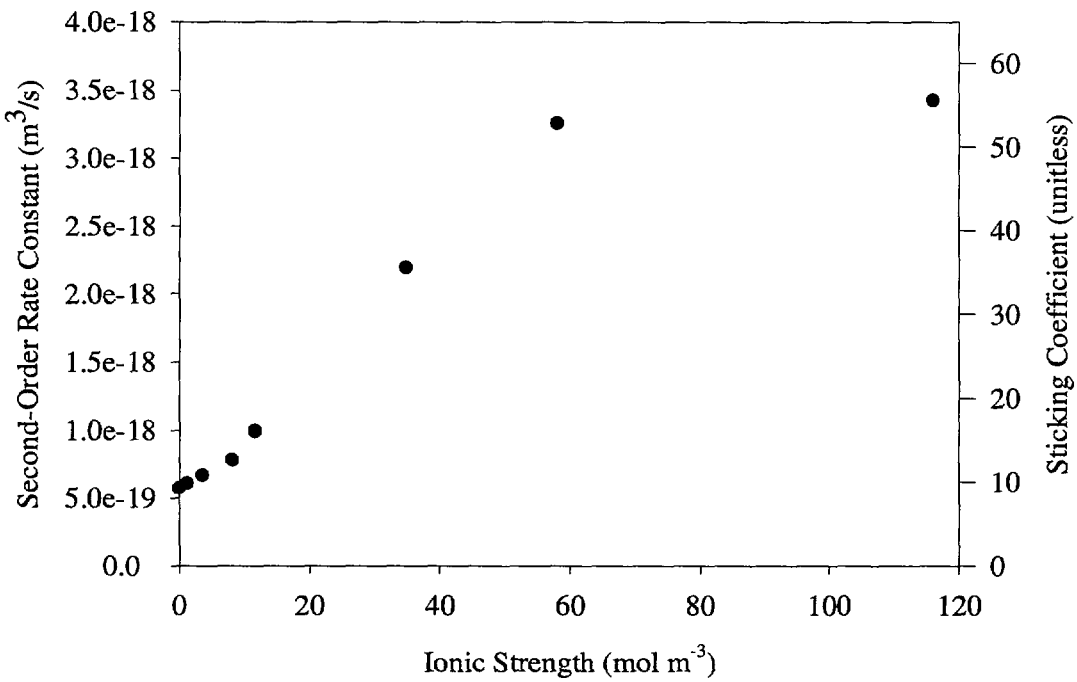

Figure 3-4
Second-Order Rate Constants and Sticking Coefficients as a Function of Ionic Strength. Regression Analysis was Conducted for data < 58 mol m^{-3}, the Approximate Critical Flocculation Concentration

Measured and calculated parameters are summarized in **Tables 3-2** and **3-3** for experiments with the conservative, non-reacting tracers and colloids, respectively. The parameters are defined as they are introduced in the following subsection and summarized as footnotes in the tables. The experiments are numbered sequentially. To facilitate comparison, the data are grouped by analyte. In all cases, full breakthrough curves were generated.

Table 3-2
Experimental Conditions and Parameters for Conservative Tracer Transport in Saturated Sand (S) and Tuff (T) Columns

Expt.	Solution	Analyte	θ[a]	PV[b] (mL)	v[c] (cm hr-1)	t_o[d] (PV)	% Recovery[e]	R[f]	P[g] (95% CI)	D[h] (95% CI)
S-1a	0X	Br^-	0.326	25.59	24.4	3.21	99.3	1.01	164 (118-210)	2.38 (1.86-3.30)
S-5	1X	Br^-	0.326	25.59	24.4	3.04	102.0	1.02	234 (175-293)	1.67 (1.33-2.23)
S-6	1X	Br^-	0.326	25.59	24.4	1.83	91.0	1.02	248 (199-296)	1.57 (1.32-1.96)
S-2	0X	PFBA	0.326	25.59	11.6	5.04	100.1	1.08	245 (226-263)	0.76 (0.71-0.82)
S-7	1X	PFBA	0.326	25.59	25.1	3.90	101.1	1.00	183 (131-235)	2.19 (1.71-3.06)
S-8	1X	PFBA	0.326	25.59	37.5	2.50	102.2	0.99	227 (152-302)	2.64 (1.99-3.94)
S-11	0X	PFBA	0.326	25.59	24.4	1.95	106.8	1.02	217 (102-331)	1.80 (1.18-3.83)
T-1	0X	PFBA	0.494	16.43	13.6	4.14	100.0	1.03	59 (39-79)	1.56 (1.16-2.36)
T-6	10X	PFBA	0.496	16.18	13.6	4.18	102.2	1.05	116 (72-159)	0.78 (0.57-1.26)
T-7	0X	PFBA	0.496	16.31	13.6	2.64	96.6	0.99	40 (25-55)	2.28 (1.66-3.65)

[a]θ, average volumetric water content
[b]PV, average pore volume of water in porous media
[c]v, average pore water velocity
[d]t_o, step input or pulse size
[e]determined by area under the effluent BTC
[f]R, retardation factor, determined by area above the BTC
[g]P, Peclet number
[h]D, hydrodynamic dispersion

Table 3-3
Experimental Conditions and Parameters for Colloid Transport in Saturated Sand (S) and Tuff (T) Columns

Expt.	Solution	θ^a	PV^b (mL)	v^c (cm hr^{-1})	t_o^d (PV)	% Recovery[e]	R^f	μ (hr^{-1})[g] (95% CI)
S-1b	0X	0.326	25.59	24.4	4.87	108.5	1.01	6×10^{-10}
S-3	0.1X	0.326	25.59	24.4	3.16	98.2	1.07	0.06 (0.02-0.09)
S-4	1X	0.326	25.59	24.4	3.04	89.3	1.01	0.18 (0.16-0.21)
S-9	10X	0.326	25.59	24.4	3.68	2.9	-	5.6 (5.4-5.8)
S-10	0X	0.326	25.59	24.4	4.41	107.0	0.95	6×10^{-10}
T-2	0X	0.496	13.63	15.81	5.37	102.1	0.87	4×10^{-9}
T-3	0.1X	0.492	13.52	15.98	7.99	100.6	0.90	5×10^{-9}
T-4	1X	0.493	13.53	15.93	7.99	87.3	0.97	0.43 (0.36-0.49)
T-5	10X	0.496	13.61	15.92	8.45	10.6	-	7.0 (6.6-7.3)
T-8	0X	0.493	13.53	15.90	8.03	102.6	0.87	6×10^{-9}

[a]θ, average volumetric water content
[b]PV, average pore volume of water in porous media
[c]v, average pore water velocity
[d]t_o, step input or pulse size
[e]determined by area under the effluent BTC
[f]R, retardation factor, determined by area above the BTC
[g]first-order rate of removal for colloid deposition on porous media

The pH of the effluent was monitored during selected experiments; there were no significant changes or trends during the experiments. Data for selected experiments are summarized in Table 3-4.

Table 3-4
Column Effluent pH for Selected Colloid Transport Experiments

Expt.	Solution	% saturation	Average pH	Standard deviation
S-1b	0x	100%	7.4	0.1
S-3	0.1x	100%	8.2	0.1
S-4	1x	100%	8.8	0.1
T-2	0x	100%	7.5	0.1
S-61-3	10x	61%	9.0	0.1
S-11-1	0x	11%	7.2	0.1

Conservative Tracer Transport

Results of the tracer experiments are shown in **Figures 3-5** and **3-6**, where the pore volume (PV) axis was truncated at 2.0 to highlight any observable differences. The BTCs appear similar for the different conditions (Table 3-2) and sharp fronts suggest "ideal" transport behavior or the absence of flow heterogeneities. Recovery was generally 100%. The low recovery for S-6 is attributed to analytical error. Recovery in excess of 100% for S-11 may be due to analytical interference by constituents leaching from the column, triggered by the change in solution matrix from 10x to 0x. Retardation factors were approximately 1.0 for 9 out of 10 experiments, as expected for conservative, non-reactive tracers (Table 3-2). The slightly higher value of 1.08 for one experiment, S-2, was not reproduced and is likely due to experimental error.

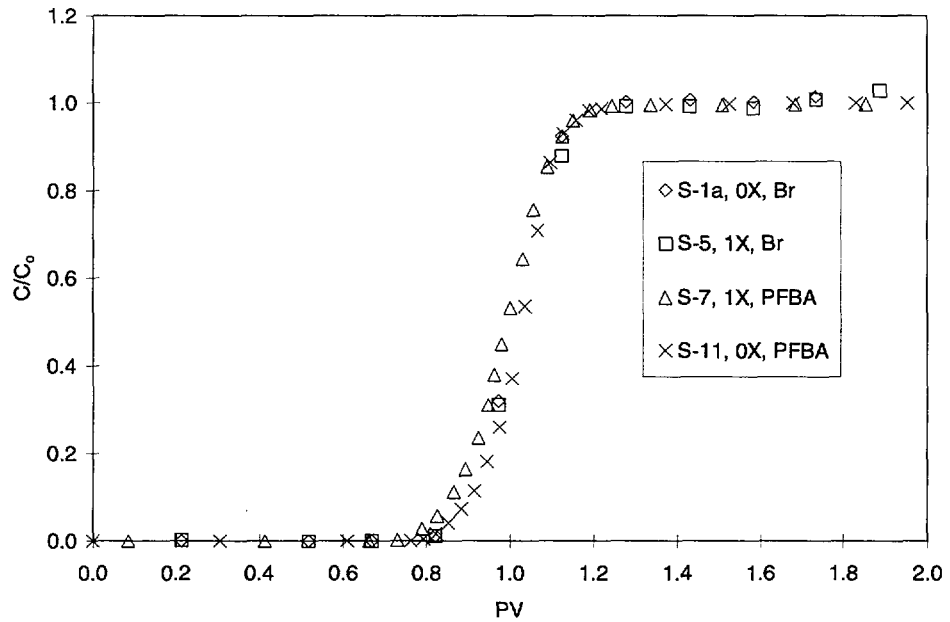

Figure 3-5
Non-interactive Tracer Transport in Quartz Sand

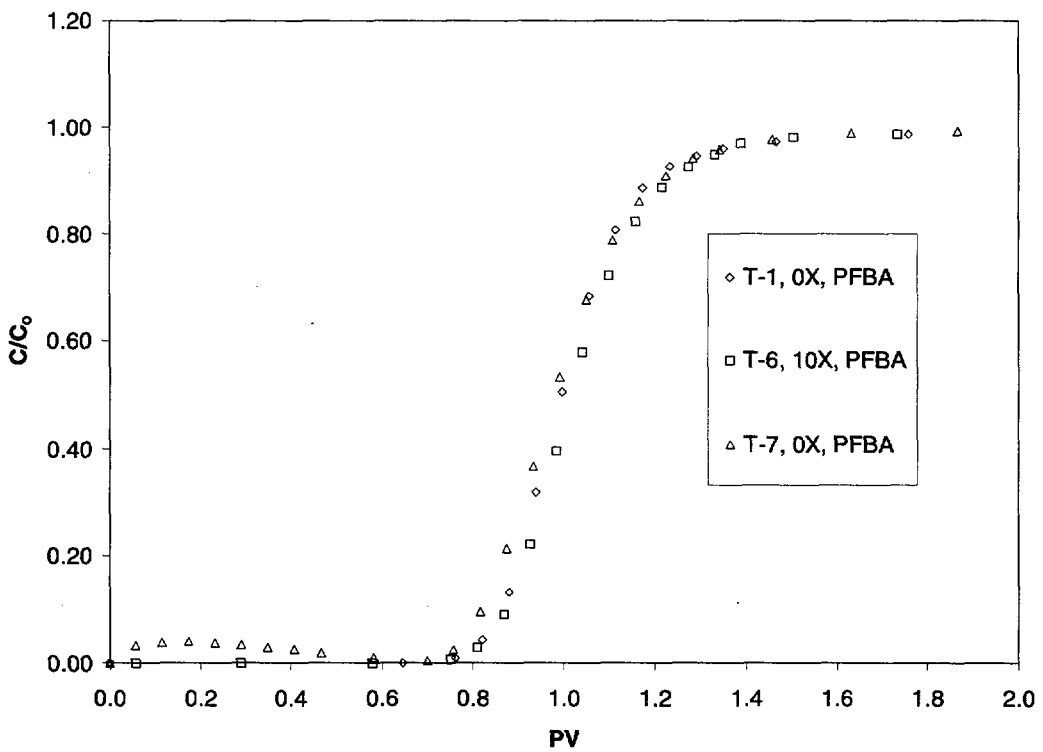

Figure 3-6
Non-interactive Tracer Transport in Yucca Mountain Tuff

The dimensionless Peclet number, P, characterizes hydrodynamic dispersion within porous media during transport. Dispersion is normalized for velocity and length, allowing comparison of measurements made under varying conditions. The Peclet number was determined with a nonlinear, least-squares, one-parameter, curve-fitting technique (CFITIM3, University of Florida) based on the Brenner solution to the convection-dispersion equation, CDE (Brenner, 1962), expressed here in dimensionless terms

$$R\frac{\partial C}{\partial T}=\frac{1}{P}\frac{\partial^2 C}{\partial Z^2}-\frac{\partial C}{\partial Z}-\mu^E C \qquad (11)$$

where R and P are as defined previously, C, T and Z are dimensionless concentration, time and distance, respectively, and μ^E is a first order decay coefficient. The decay term is zero for conservative tracers and describes irreversible deposition of the colloids on the porous media.. The dimensionless terms are further defined in **Table 3-5**. The model fits overlie the experimental BTCs, but were omitted from **Figures 3-5** and **3-6** because they obscured the data.

Table 3-5
Definition of Dimensionless Transport Parameters (after Toride et al., 1995)

Parameters	T	Z	P	R	C	μ^E
Expressions	$\frac{vt}{L}$	$\frac{x}{L}$	$\frac{vL}{D}$	$1+\frac{\rho_b K_d}{\theta}$	$\frac{c}{c_o}$	$\frac{L\mu_l}{v}$

In **Table 3-5**, t is time (hr), x is distance (cm), D is hydrodynamic dispersion (cm^2/hr), K_d is the equilibrium sorption constant, μ is the first-order decay term (hr^{-1}) where the subscript l represents the liquid phase; all other terms are as defined previously. The first-order decay term presented here using conventional transport terminology, μ_l, is equivalent to the pseudo-first-order removal rate coefficient (equation 1) that was defined for colloid removal by deposition, k_d.

Peclet numbers were somewhat lower for the tuff than the sand column; the decrease from 59 to 40 between the first and penultimate experiment on the tuff was not statistically significant. Ionic strength had no effect on retardation, retention, or dispersion of the tracers, and hydrodynamic conditions did not change appreciably after colloids were displaced, and in some cases deposited, on the sediment. The tracer experiments provide an indicator of column performance, particularly as multiple experiments were performed on the same column. The results for S-11 indicate that hydrodynamic dispersion did not change following the colloid transport experiments (S-1b-S-10).

Colloid Transport and Retention

The effect of ionic strength on colloid mobility is illustrated in **Figures 3-7** and **3-8** and quantified in **Table 3-3**. The results for 0x (de-ionized) water serve as an important control, indicating mobility at the velocity of the aqueous solution (R = 1). Recovery was 100% (or greater) indicating no retention on the sediment. Recall that the pH for the 0x solution is lower

than that of the other synthetic J-13 solutions, possibly increasing the hydrophobic character of the colloid surface, which would result in retardation of the colloids. This effect was not observed, indicating that the lower pH for the 0x solution did not change the transport behavior. Although the sand column was pre-equilibrated with > 35 pore volumes of 0x solution prior to colloid application, there is clearly an interference with the colloid analysis (S-1b) resulting in >100% recovery and $c/c_0 > 1.0$. This is likely due to the absence of cations and anions in solution and was not observed with the synthetic J-13 solutions. Note that the effect had subsided with the final experiment in the 0x matrix (S-10) and was not observed for the tuff. The conditions for S-10 were identical to those of S-1b; the results (Table 3-3) indicate that performing multiple experiments on the columns did not change colloid deposition and transport.

Colloid deposition during transport was modeled using an analytical solution to the CDE, CXTFIT, version 2.1 (Toride et al., 1995). A one-parameter curve-fit was used to determine μ^E from BTC data, with the exception of S-9 and T-5, where both R and μ^E were determined by curve-fitting. As mentioned previously, due to the small mass recovered in the effluent, and lack of a clear plateau for the BTC, estimates of R based on the area above the BTC or center-of-mass may not be valid. Values of P were fixed to those determined with conservative tracers, recognizing that due to the size difference, dispersion of the colloid may be less than that of the tracers. Given the limited dispersion in these systems, the difference was ignored. For 0x and 0.1x, colloid deposition was essentially zero (S-1b, S-10, T-2, T-3, T-8). The similarity in colloid transport for 0x and 0.1x solutions indicates that the increase in pH from 7.6 for 0x to 8.5 for 0.1x did not affect colloid transport or deposition. For ionic strengths greater than 0.1x, the removal rate coefficient (μ_l or k_d) increased with increasing ionic strength. Agreement between the model and experimental data indicate that colloid deposition during transport can be described as a pseudo first-order process.

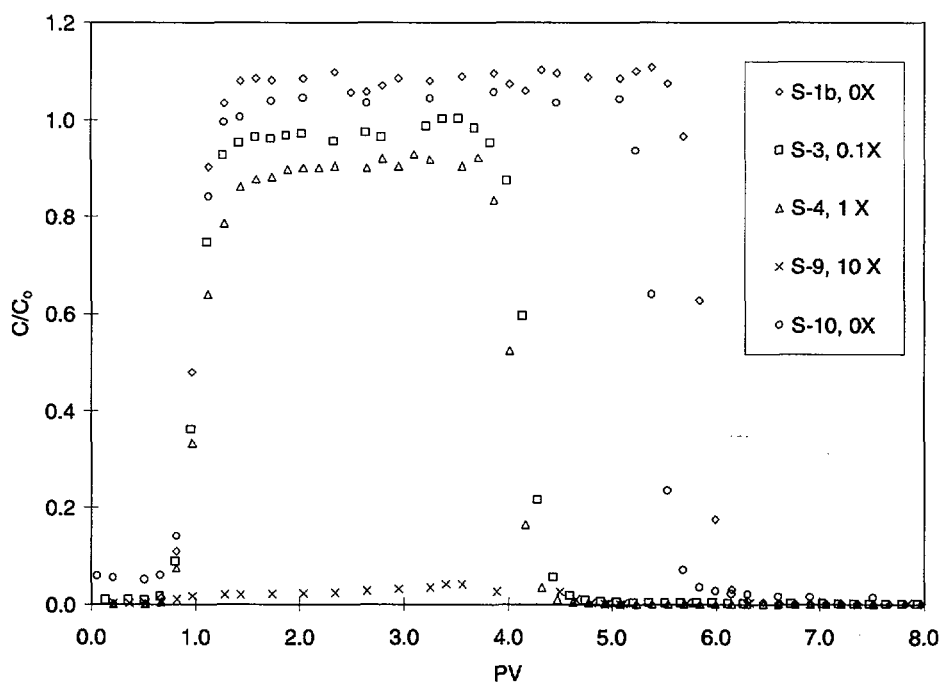

Figure 3-7
Transport and Deposition of 280 nm Colloids in Quartz Sand

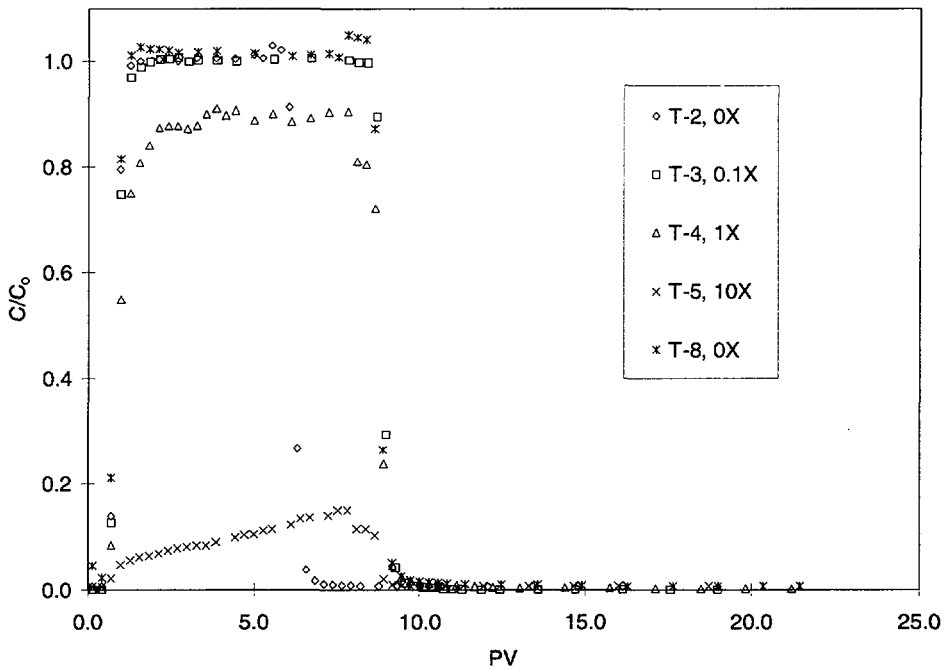

Figure 3-8
Transport and Deposition of 280 nm Colloids in Yucca Mountain Tuff

A systematic increase in colloid retention on the sediment with increasing ionic strength is indicated by the lower plateau of the BTCs, lower % recovery of colloids in the column effluent, and increase in the rate coefficient for colloid removal (**Table 3-3**). The pH for the 0.1x, 1x, and 10x solutions was similar, indicating that the effect is due to ionic strength, rather than a change in pH. For the limited conditions evaluated, the mass fraction of colloids retained appears to increase linearly with increasing ionic strength (**Figure 3-9**).

Although ionic strength affected deposition, the velocity of the *mobile* colloids did not vary greatly from that of the aqueous solution, i.e., R was approximately equal 1.0 for colloids in the effluent. Retardation of the colloids was ~0.9 through the tuff at low ionic strength. Physical exclusion from smaller pores that remain accessible to water and dissolved solutes could result in R <1, however, this physical effect and would be independent of ionic strength. Anion exclusion is an alternative mechanism that is more consistent with the observation primarily at low ionic strength.

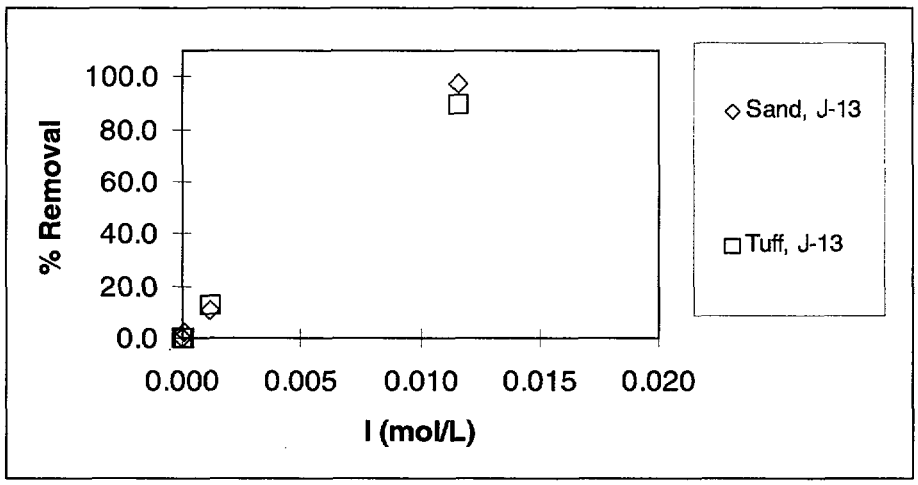

Figure 3-9
Colloid Deposition during Transport in Sand and Tuff

Transport Experiments in Unsaturated Columns

Results of unsaturated transport experiments are also expressed as breakthrough curves (BTCs), depicting the dimensionless effluent concentration (c/c_0) as a function of cumulative pore volumes eluted. The percent recovery of the analyte in the effluent was based on the area under the BTC compared with the measured step input. Values of the retardation factor, R, were determined based on the mathematical first moment (Valocchi, 1985) when it was not appropriate to use the area above the BTC method, i.e., lack of a clear plateau for the effluent BTC.

Measured and calculated parameters are summarized in **Tables 3-6** and **3-7** for experiments with the non-reactive tracers and colloids, respectively. The experiments are numbered sequentially. The percent moisture content is also indicated to distinguish between higher and lower unsaturated moisture conditions. For example, the second experiment at 61% moisture saturation on the sand column is designated as "S-61-2" ("a" and "c" at the end of the "S-61-2" essentially refers to two replicates). In all cases, full breakthrough curves were generated.

Table 3-6
Experimental Conditions and Parameters for Conservative Tracer Transport in Unsaturated Sand (S) and tuff (T) Columns

Expt.	Solution	Analyte	θ[a]	PV[b] (mL)	v[c] (cm hr-1)	t_o[d] (PV)	% Recovery[e]	R[f]	P[g] (95% CI)	D[h] (95% CI)
S-61-2a	0x	Br^-	0.289	27.61	17.38	2.16	97.2	1.16	26 (18-33)	4.0 (3.1-5.8)
S-61-2c	0x	Br^-	0.266	24.54	18.94	2.34	95.4	1.05	24 (17-30)	4.8 (3.8-6.7)
T-71-1c	0x	Br^-	0.383	36.54	13.14	2.99	100.0	1.02	8.4 (6.6-10.2)	10.9 (9.0-13.8)
S-11-4a	0x	Br^-	0.039	3.70	64.94	3.27	87.5	0.77	0.37 (0.13-0.62)	1078 (656-3033)
S-11-4c	0x	Br^-	0.040	3.84	62.55	3.66	81.1	0.94	0.86 (0.17-1.6)	425 (236-2124)
T-17-1c	0x	Br^-	0.091	8.71	27.56	4.52	92.3	0.71	0.21 (0.12-0.31)	742 (512-1349)

[a]θ, average volumetric water content
[b]PV, average pore volume of water in porous media
[c]v, average pore water velocity
[d]t_o, step input or pulse size
[e]determined by area under the effluent BTC
[f]R, retardation factor, determined by center-of-mass
[g]P, Peclet number
[h]D, hydrodynamic dispersion

Table 3-7
Experimental Conditions and Parameters for Colloid Transport in Unsaturated Sand (S) and tuff (T) Columns

Expt.	Solution	θ[a]	PV[b] (mL)	v[c] (cm hr^{-1})	t_o[d] (PV)	% Recovery[e]	R[f] (AAC)	R[g] (COM)
S-61-1a	0x	0.233	22.20	16.19	4.18	103.6	0.90	1.09
S-61-1c	0x	0.192	18.28	16.65	5.87	101.0	0.88	1.05
S-61-3a	0.1x	0.204	19.44	24.69	3.80	97.3	1.01	1.14
S-61-3c	0.1x	0.234	22.29	21.54	3.45	97.4	1.13	1.07
S-61-4a	1x	0.204	19.43	24.70	3.11	96.1	1.04	1.09
S-61-4c	1x	0.208	19.80	24.24	3.11	95.1	1.09	1.06
S-61-5a	10x	0.119	11.33	42.38	5.32	8.2	-	1.21
S-61-5c	10x	0.211	20.15	23.82	3.20	3.7	-	0.93
T-61-2c	0x	0.329	31.38	15.30	5.31	101.0	0.75	0.85
T-59-3c	0.1x	0.320	30.57	15.70	6.20	92.0	0.75	0.83
T-58-4c	1x	0.314	30.00	16.00	5.57	71.5	-	0.89
T-58-5c	10x	0.310	26.92	16.20	6.06	4.2	-	1.91

[a]θ, average volumetric water content
[b]PV, average pore volume of water in porous media
[c]v, average pore water velocity
[d]t_o, step input or pulse size
[e]determined by area under the effluent BTC
[f]R, retardation factor, determined by area above the BTC
[g] retardation factor, determined by center-of-mass
[h]first-order rate of removal for colloid deposition on porous media

Table 3-7 (continued). Unsaturated colloids

Expt.	Solution	θ	PV (mL)	v (cm hr^{-1})	t_o (PV)	% Recovery	R (AAC)	R (COM)	μ (hr^{-1}) (95% CI)
S-11-1a	0x	0.036	3.41	70.46	12.40	83.5	0.90	0.77	
S-11-1c	0x	0.039	3.70	64.87	11.50	77.0	0.96	0.95	
S-11-2a	0x	0.037	3.57	67.23	4.96	81.5	0.79	0.68	
S-11-2c	0x	0.041	3.94	60.90	4.11	98.5	0.56	1.09	
S-11-5a	0.1x	0.038	3.62	66.23	5.37	82.4	0.93	0.83	
S-11-5c	0.1x	0.039	3.70	64.90	4.46	76.9	0.67	0.73	
S-11-6a	1x	0.038	3.61	66.52	5.31	47.2	0.50	0.76	
S-11-6c	1x	0.038	3.62	66.23	4.27	48.6	0.34	1.07	
T-18-2c	0x	0.095	9.05	26.53	6.76	62.8	-	0.81	
T-18-3c	0.1x	0.095	9.03	26.58	6.32	58.3	-	0.33	
T-17-4c	1x	0.093	8.84	27.15	6.65	25.6	-	1.33	
T-16-5c	10x	0.087	8.27	29.02	6.86	11.1	-	1.54	

[a]θ, average volumetric water content
[b]PV, average pore volume of water in porous media
[c]v, average pore water velocity
[d]t_o, step input or pulse size
[e]determined by area under the effluent BTC
[f]R, retardation factor, determined by area above the BTC
[g] retardation factor, determined by center of mass
[h]first-order rate of removal for colloid deposition on porous media

Conservative Tracer Transport

Results of the tracer experiments are shown in **Figures 3-10** and **3-11**, for two unsaturated moisture conditions on sand and tuff sediments, respectively.

The dimensionless Peclet number, P, was determined as above, using a nonlinear, least-squares, one-parameter, curve-fitting technique (CFITIM3, University of Florida) based on the Brenner solution to the convection-dispersion equation, CDE (Brenner, 1962), where the terms are defined above, and in **Table 3-5**.

As for the saturated condition, Peclet numbers were lower for the tuff than the sand column indicating greater dispersion. The results also show increased dispersion or hydrodynamic heterogeneity with decreasing moisture content. This is consistent with the development of stagnant or immobile water regions in unsaturated porous media. The of coupling of physical nonequilibrium processes such as mass transfer between regions of mobile and immobile water with chemical reaction processes such as colloid deposition, has not yet been addressed. For this reason, parameter estimates of colloid deposition rates are not reported in Table 3-7, however, the % recovery quantifies the extent of colloid deposition.

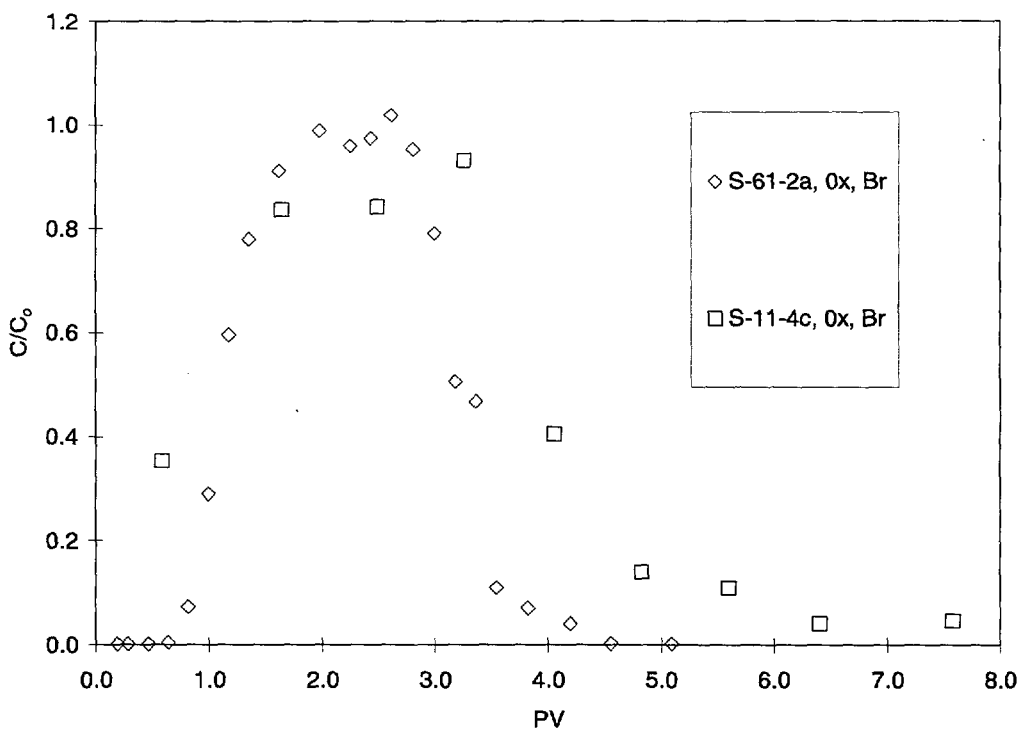

Figure 3-10
Non-interactive Tracer Transport in Quartz Sand at 61% and 11% Moisture Saturation

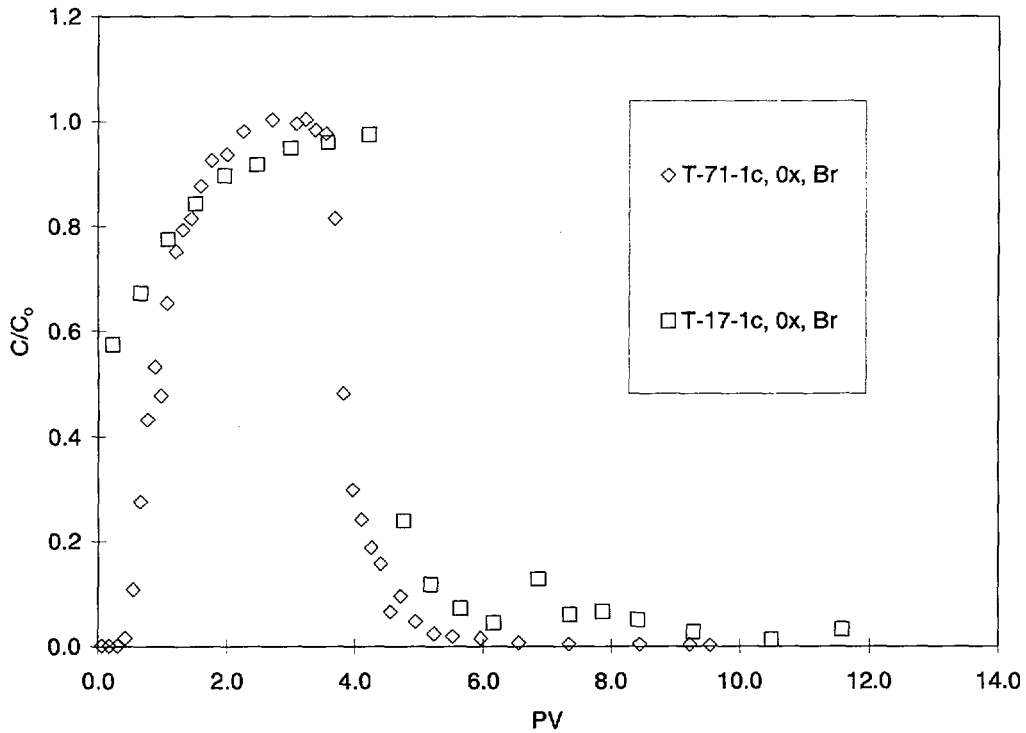

Figure 3-11
Non-interactive Tracer Transport in Yucca Mountain Tuff at 71% and 17% Moisture Saturation

Colloid Transport and Retention

The effect of ionic strength on colloid mobility at two unsaturated moisture contents is illustrated in **Figures 3-12** through **3-15** and quantified in **Table 3-7**. Retardation factors in Table 3-7 were calculated using both the area above the curve (AAC) method (Nkedi-Kizza et al., 1987) and based on the center-of-mass (COM) of the BTC (Valocchi, 1985). The results for ~ 60% moisture saturation in sand and are similar to transport and retention in saturated sediments. Once again, the results for 0x indicate colloid mobility at the velocity of the aqueous solution (R = 1), and 100% recovery of the applied colloids.

A systematic increase in colloid deposition on the sediment with increasing ionic strength is indicated by the lower maximum of the BTCs and lower % recovery of colloids in the column effluent (**Table 3-7**). For each ionic strength, the results also show increased colloid deposition at the lower water content, indicating that physical properties also play a role in colloid removal.

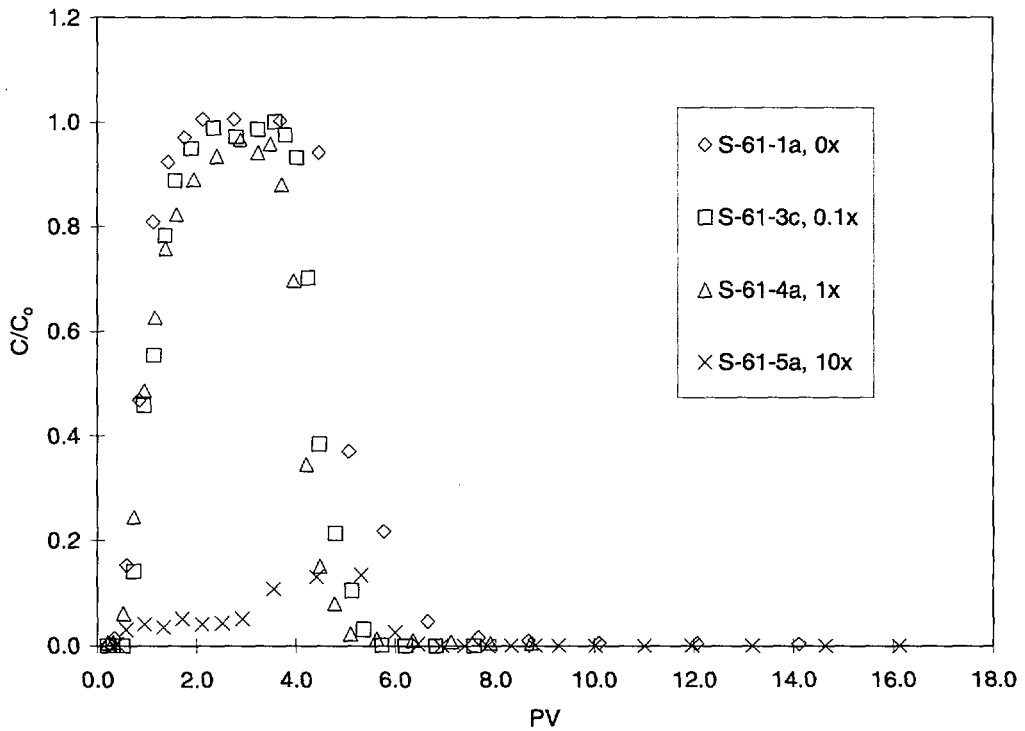

Figure 3-12
Transport and Deposition of 280 nm Colloids in Quartz Sand at 61% Moisture Saturation

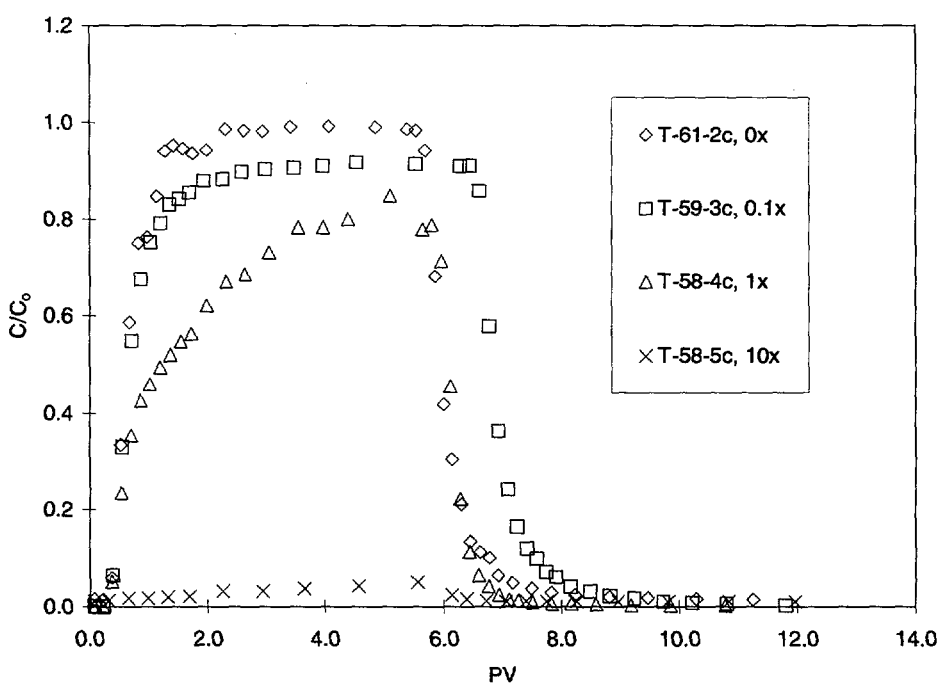

Figure 3-13
Transport and Deposition of 280 nm Colloids in Tuff at 58% Moisture Saturation

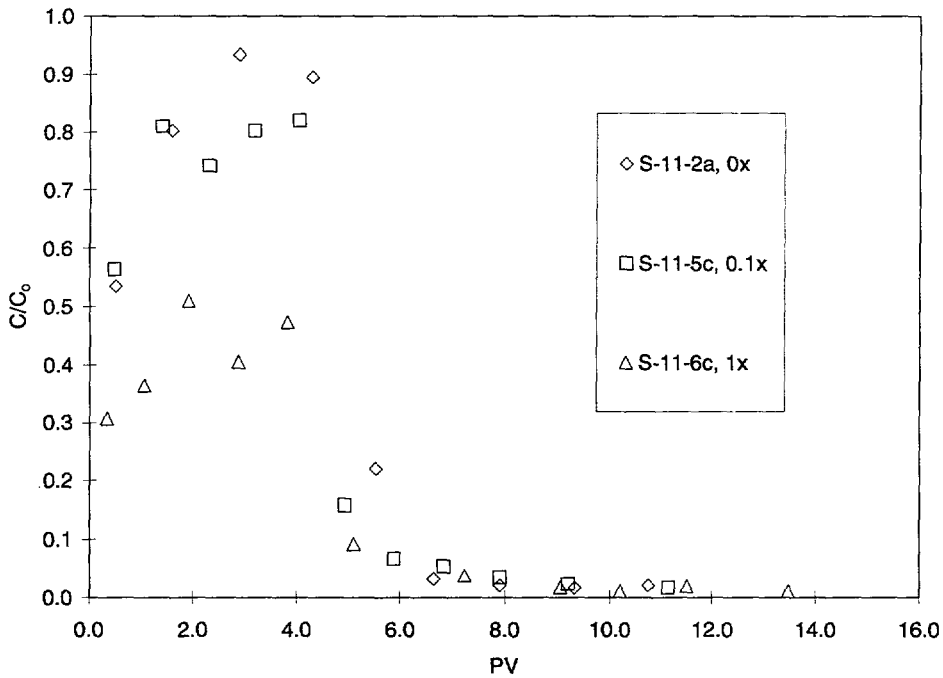

Figure 3-14
Transport and Deposition of 280 nm Colloids in Quartz Sand at 11% Moisture Saturation

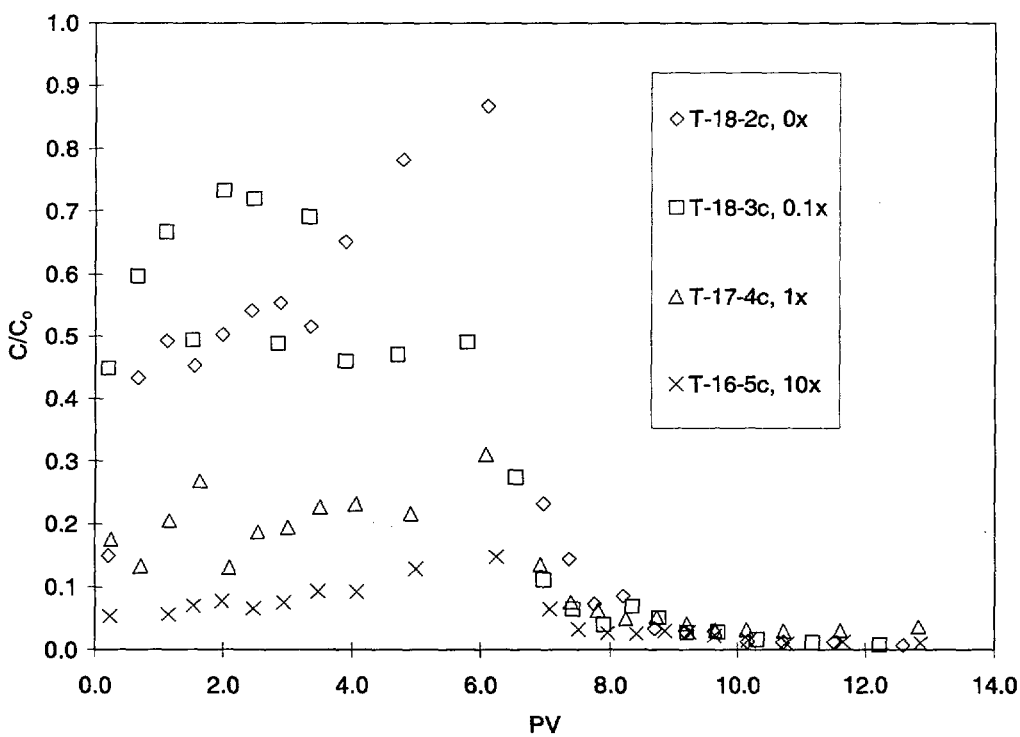

Figure 3-15
Transport and Deposition of 280 nm Colloids in Tuff at 17% Moisture Saturation

Israelachvili, J. (1991) Intermolecular and surface Forces. 2nd Edition, Academic Press, London, England.

Kaplan, D. I., Bertsch, P. M., Adriano, D. C., and Miller, W. P. (1993). Soil-Borne Mobile Colloids As Influenced by Water Flow and Organic Carbon. Environ. Sci. Technol., 27 (6), 1193-1200.

Kaplan, D. I., Bertsch, P. M., Adriano, D. C., and Miller, W. P. (1995). Facilitated Transport of Contaminant Metals Through an Acidified Aquifer. Ground Water, 33 (5), 707-717.

Kaplan, D.I., C. W. Lindenmeier, and R. J. Serne. 1996. "Moisture Dependency of Solute Adsorption Constants." AGU 1996 Fall Meeting. San Francisco, CA. Dec 11 - 16. American Geophysical Union, Washington, DC. pp. F274.

Levy, S. S. (1992) Natural Gels in the Yucca Mountain area, Nevada, USA. Applied Clay Science. 7:79-85.

Kerrisk, J. 1987. "Groundwater Chemistry at Yucca Mountain, Nevada, and Vicinity," Los Alamos National Laboratory. LA-10929-MS. Los Alamos National Laboratory, Los Alamos, NM.

Kersting, A. B., and A. Brachmann. 1999. Identification of groundwater colloids from the Nevada Test Site. Presented at Migration 99: Chemistry and Migration Behavior of Actinides and Fission Products in the Geosphere. Incline Village, Lake Tahoe, NV, September 26 – October 1, 1999.

Kersting, A. B., Efurd, D. W. Finnegan, D. L., Rokop, D. J., Smith, D. K. and Thompson, J. L. (1999). Migration of plutonium in ground water at the Nevada Test Site. Nature, 397: 56-59.

Levy, S. S. 1992. Applied Clay Science. 7:79-85.

Kingston, W. L., and M. Whitbeck. 1991. "Characterization of Colloids Found in Various Groundwater Environments in Central and Southern Nevada. #45083, Los Alamos National Laboratory, Los Alamos, New Mexico.

Lindenmeier, C.W., R. J. Serne, J. L. Conca, A. T. Owen, and M. I. Wood.(1995). "Solid Waste Leach Characteristics and Contaminant-sediment Interactions Volume 2: Contaminant Transport Under Unsaturated Moisture Contents." PNL-10722, Pacific Northwest National Laboratory, Richland, WA.

Mann, F. M. (1998). Hanford Immobilized Low-Activity Tank Waste Performance Assessment. DOE/RL-97-69, UC-2050.

McCarthy, J. F., and J. M. Zachara. 1989. Subsurface transport of contaminants. Environ. Sci. Technol., 23:496-502.

McGraw, M.A. 1996. "Effect of Colloid Size, Colloid Hydrophobicity, and Volumetric Water Content on the Transport of Colloids Through Porous Media." Ph.D. Dissertation. University of California - Berkeley, Berkeley, CA.

McGraw, M.A., A Wolfsberg, and G. Roemer. (1998). Significant Mechanisms and Issues for Development of a Fractured, Saturated-Zone, Colloid Transport Model. Presented at the Colloid Facilitated Transport Workshop, July 20 – 21, 1998. Las Vegas, Nevada.

Meijer, A. (1990). Yucca Mountain Project far-field sorption studies and data needs. Los Alamos National Laboratory Report LA-11671-MS, UC-510, Los Alamos.

Meijer, A. (1992). A Strategy for the Derivation and Use of Sorption coefficients in Performance Assessment Calculations for the Yucca Mountain Site, in Proceedings of the DOE/Yucca Mountain Site Characterization Project Radionuclide Adsorption Workshop at Los Alamos National Laboratory, September 11-12, 1990, Lost Alamos National Laboratory Report, LA-12325-C, NNA.920819.0077.

Minai, Y., Choppin, G. R., and Sisson, D. H. (1992). Humic material in well water from the Nevada Test Site. Radiochimica Acta, 56, 195-199.

Nimmo, J.R., K. C. Akstin, and K. A. Mello. (1992) Improved Apparatus for Measuring Hydraulic Conductivity at Low Water Content. Soil Sci. Soc. Am J. 56(6):1758-1761.

Nimmo, J.R., D. A. Stonestrom, and D. C. Akstin. (1994) The Feasibility of Recharge Rate Determinations Using the Steady-State Centrifuge Method. Soil Sci. Soc. Am. J. 58:49-56.

Nkedi-Kizza, P., P.S.C. Rao, and A.G. Hornsby. 1987. Influence of organic cosolvents on leaching of hydrophobic organic chemicals through soils. Environ. Sci. Technol. 21:1107-1111.

Ogard, A. 1987. "Importance of Radionuclide Transport by Particulates Entrained in Flowing Groundwaters." In *Groundwater Chemistry at Yucca Mountain, Nevada, and Vicinity." J.* F. Kerrisk, Los Alamos National Laboratory. LA-10929-MS, Los Alamos National Laboratory, Los Alamos, NM. pp. 481-488.

O'Melia, C. R. (1978) Coagulation in Wastewater Treatment. In: The Scientific Basis of Flocculation, K. J. Ives (Ed.) Sijthoff and Noordhoff. pp. 219-268. Alphen aan den Rijn, The Netherlands.

Ramsay, J.D.F. 1988. "The Role of Colloids in the Release of Radionuclides from Nuclear Waste." Radiochimica Acta. 44/45:165-170.

Relyea, J. F. 1982. Theoretical and Experimental Considerations for the Use of the Column Method for Determining Retardation Factors. Radioactive Waste Management and the Nuclear Fuel Cycle. 3(2):151-166.

Ruckenstein, E., and D. C. Prieve. (1976). Adsorption and Desorption of Particles and Their Chromatographic Separation. Amer. Inst. Chem. Eng. J. 22:276-283.

Ryan, J. N., and P. M. Gschwend. 1994. Effect of Solution Chemistry on Clay Colloid Release from an Iron Oxide-Coated Aquifer Sand. Environ. Sci. Technol. 28:1717-1726.

Shields, K.D. 1995. "Comparison of Soil Physical Properties for Carbon Tetrachloride and Water Using the UFA Method." M.S. Thesis, Washington State University, Pullman, WA.

Stockman, C. 1998. Colloid Modeling in the TSPA-VA. Presented at the Colloid Facilitated Transport Workshop, July 20 – 21, 1998. Las Vegas, Nevada.

Stumm, W., and J.J. Morgan. 1996. Aquatic Chemistry, 3rd ed., Wiley-Interscience Publication, New York.

Sumner, M. E. (1993). Sodic Soils: New Perspectives. Aust. J. Soil Res., 31, 683-750.

Thompson, J.L. 1989. Actinide Behavior on Crushed Rock Columns. Journal of Radioanalytical and Nuclear Chemistry. 130(2):353-364.

Tien, C. 1989. *Granular Filtration of Aerosols and Hydrosols.* Butterworths, Boston.

Tobiason, J. E. (1989). Chemical Effects on the Depositions of Non-Brownian Particles. Colloids and Surfaces, 39, 53-77.

Toride, N., F.J. Leij, and M. Th. van Genuchten. 1995. The CXTFIT Code for Estimating Transport Parameters from Laboratory or Field Tracer Experiments, Version 2.1, Research Report No. 137, U.S. Salinity Laboratory, Agricultural Research Service, U.S. Department of Agriculture, Riverside, CA.

Triay, I., A. Simmons, S. Levy, J. Nuttall, B. Robinson, W. Stenkampf, B. Vianni, and S. Nelson. 1994. "Colloid-Facilitated Radionuclide Transport at Yucca Mountain." LA-12779-MS. Los Alamos National Laboratory, Los Alamos, NM.

Triay, I., C. Degueldre, A. O. Wistrom, C. R. Cotter, and W. W. Lemons. 1996. "Progress Report on Colloid-Facilitated Radionuclide Transport at Yucca Mountain. Yucca Mountain Site Characterization Program Milestone No. 3383." LA-12959-MS. Los Alamos National Laboratory, Los Alamos, NM.

TRW (1995). Total system performance assessment – 1995. An evaluation of the potential Yucca Mountain repository. TRW Report No. 01717-2200-00136, Rev. 01., Las Vegas.

Valocchi, A. L., 1985. Validity of the local equilibrium assumption for modeling sorbing solute transport through homogeneous soils, *Water Resour. Res., 21*, 808-820.

van Olphen, H. (1977) Clay Colloid Chemistry. Wiley-Interscience Publication, New York.

Wan, H. and Tokunaga, T. (1997). Film Straining of Colloids in Unsaturated Porous Media: Conceptual Model and Experimental Testing. Environmental Science & Technology, 31, 2413-2420.

Wan, J. and Wilson, J. L. (1994). Visualization of the role of the gas-water interface on the fate and transport of colloids in porous media. Water Resources Research, 30(1), 11-23.

Wan, J. and Wilson, J. L. (1994). Colloid transport in unsaturated porous media. Water Resources Research, 30(4), 857-864.

Zhong, W. Z., A.T. Lemley, R.J. Wagenet. 1986. Quantifying pesticide adsorption and degradation during transport through soil to groundwater. *In* Evaluation of Pesticides in Ground Water, W.Y. Garner, R.C. Honeycutt, and H.N. Nigg, eds., ACS Symposium Series 315, American Chemical Society, Washington, DC., pp 61-77.

Target:
Nuclear Power

About EPRI

EPRI creates science and technology solutions for the global energy and energy services industry. U.S. electric utilities established the Electric Power Research Institute in 1973 as a nonprofit research consortium for the benefit of utility members, their customers, and society. Now known simply as EPRI, the company provides a wide range of innovative products and services to more than 1000 energy-related organizations in 40 countries. EPRI's multidisciplinary team of scientists and engineers draws on a worldwide network of technical and business expertise to help solve today's toughest energy and environmental problems.

EPRI. Powering Progress

© 1999 Electric Power Research Institute (EPRI), Inc. All rights reserved. Electric Power Research Institute and EPRI are registered service marks of the Electric Power Research Institute, Inc. EPRI. POWERING PROGRESS is a service mark of the Electric Power Research Institute, Inc.

Printed on recycled paper in the United States of America

TR-110546

EPRI • 3412 Hillview Avenue, Palo Alto, California 94304 • PO Box 10412, Palo Alto, California 94303 • USA
800.313.3774 • 650.855.2121 • askepri@epri.com • www.epri.com